



**HAL**  
open science

## **Liver precursor cells increase hepatic fibrosis induced by chronic carbon tetrachloride intoxication in rats.**

Marie-Noële Chobert, Dominique Couchie, Agnès Fourcot, Elie-Serge Zafrani, Yannick Laperche, Philippe Mavier, Arthur Brouillet

### ► To cite this version:

Marie-Noële Chobert, Dominique Couchie, Agnès Fourcot, Elie-Serge Zafrani, Yannick Laperche, et al.. Liver precursor cells increase hepatic fibrosis induced by chronic carbon tetrachloride intoxication in rats.: LPC aggravates liver CCl4-induced fibrosis. *Laboratory Investigation*, 2012, 92 (1), pp.135-50. 10.1038/labinvest.2011.143 . inserm-00665625

**HAL Id: inserm-00665625**

**<https://inserm.hal.science/inserm-00665625>**

Submitted on 1 Jul 2012

**HAL** is a multi-disciplinary open access archive for the deposit and dissemination of scientific research documents, whether they are published or not. The documents may come from teaching and research institutions in France or abroad, or from public or private research centers.

L'archive ouverte pluridisciplinaire **HAL**, est destinée au dépôt et à la diffusion de documents scientifiques de niveau recherche, publiés ou non, émanant des établissements d'enseignement et de recherche français ou étrangers, des laboratoires publics ou privés.

**LIVER PRECURSOR CELLS INCREASE HEPATIC FIBROSIS INDUCED BY CHRONIC CARBON TETRACHLORIDE INTOXICATION IN RAT**

Marie-Noele CHOBERT<sup>1,2</sup> #, Dominique COUCHIE<sup>2,3</sup> #, Agnès FOURCOT<sup>2</sup>, Elie-Serge ZAFRANI<sup>1,2,4</sup>, Yannick LAPERCHÉ<sup>1,2</sup>, Philippe MAVIER<sup>2</sup>, Arthur BROUILLET<sup>1,2</sup>

(1) INSERM, UMR-S-955, Equipe 17, Créteil, France

(2) Université Paris-Est Créteil, France

(3) INSERM, UMR-S-955, Equipe 21, Créteil, France

(4) AP-HP, Groupe Hospitalier Henri Mondor, Département de Pathologie, Créteil, France

# Both authors contributed equally to this work.

Correspondence :

Arthur BROUILLET, PhD, INSERM U955 Equipe 17,

Institut Mondor de Recherche Biomédicale, Créteil, F-94010, FRANCE

Tel : +33 (0)1 49 81 35 37 Fax : +33 (0)1 48 98 09 08

e-mail : [arthur.brouillet@inserm.fr](mailto:arthur.brouillet@inserm.fr)

Short running title : LPC aggravates liver CCl<sub>4</sub>-induced fibrosis

Pages of text: 27

Tables: 1

Black and white or grayscale figures: 1

Color figures: 6

Table of Contents Categories for Laboratory Investigation:

- 1- Oral, Gastrointestinal, Hepatic & Pancreatic Systems
- 2- Blood, Lymphatics, Immune System, Stem Cells
- 3- Development, Matrix Biology and Aging

**Abstract**

Hepatic fibrosis, the major complication of virtually all types of chronic liver damage, usually begins in portal areas, and its severity has been correlated to liver progenitor cells (LPC) expansion from periportal areas, even if the primary targets of injury are intralobular hepatocytes. The aim of this study was to determine the potential fibrogenic role of LPC, using a new experimental model in which rat liver fibrosis was induced by chronic carbon tetrachloride (CCl<sub>4</sub>) administration for 6 weeks, in combination with chronic acetylaminofluorene treatment (AAF), which promotes activation of LPC compartment. Treatment with CCl<sub>4</sub> alone caused a significant increase in serum transaminase activity as well as liver fibrosis initiating around central veins and leading to formation of incomplete centro-central septa with sparse fibrogenic cells expressing  $\alpha$ -smooth muscle actin ( $\alpha$ SMA). In AAF/CCl<sub>4</sub>-treated animals, the fibrogenic response was profoundly worsened, with formation of multiple porto-central bridging septa leading to cirrhosis, whereas hepatocellular necrosis and inflammation were similar to those observed in CCl<sub>4</sub>-treated animals. Enhanced fibrosis in AAF/CCl<sub>4</sub> group was accompanied by ductule forming LPC expanding from portal areas,  $\alpha$ SMA-positive cells accumulation in the fibrotic areas and increased expression of hepatic collagen type 1, 3 and 4 mRNA. Moreover, CK19-positive LPC expressed the most potent fibrogenic cytokine transforming growth factor- $\beta$  (TGF $\beta$ ) without any expression of  $\alpha$ SMA, desmin or fibroblast-specific protein-1, demonstrating that LPC did not undergo an epithelial-mesenchymal transition. In this new experimental model, LPC, by expressing TGF $\beta$ , contributed to the accumulation of  $\alpha$ SMA-positive myofibroblasts in the ductular reaction leading to enhanced fibrosis but also to disease progression and to a fibrotic pattern similar to that observed in human.

**List of abbreviations:**  $\alpha$ SMA,  $\alpha$ -smooth muscle actin; AAF, acetylaminofluorene; AFP,  $\alpha$ -fetoprotein; ALT, alanine aminotransferase; CCl<sub>4</sub>, carbon tetrachloride; CK19, cytokeratin 19; CCR2, chemokine C-C motif receptor 2; EMT, epithelial-mesenchymal transition; HSC, hepatic stellate cells; LPC, liver progenitor cells; TGF $\beta$ , transforming growth factor- $\beta$ ; TNF $\alpha$ , tumor necrosis factor- $\alpha$ .

**Keywords:** fibrosis, liver progenitor cells, TGF $\beta$ , epithelial-mesenchymal transition.

Hepatic fibrosis is the major complication of virtually all types of chronic liver damage (e.g. viral, alcoholic liver disease- or non-alcoholic fatty liver disease). In human, fibrosis that ultimately leads to cirrhosis initiates predominantly in the portal areas even though the primary targets of injury are hepatocytes within the lobule.<sup>1</sup> Impairment of the replicative capacity of most remnant hepatocytes induces an alternate regenerative process from liver progenitor cells (LPC). These cells (also called oval cells in rodent) are located in the most peripheral branches of the biliary tree (canal of Hering).<sup>2</sup> Once activated, LPC proliferate in the portal region and migrate into the hepatic lobule where they undergo further differentiation into hepatocytes or bile duct cells to repopulate the hepatic parenchyma.<sup>3,4</sup> This proliferative response characterized by the appearance of bile-duct-like structures in human is referred to atypical ductular reaction.<sup>5</sup> LPC have been of increasing interest in latest years since they could play a role not only in regeneration but also in fibrogenesis and carcinogenesis.<sup>6</sup> In experimental models and various human liver diseases, LPC expand in close proximity to  $\alpha$ -smooth muscle actin ( $\alpha$ SMA)-positive cells deriving from either sinusoidal hepatic stellate cells (HSC) or portal fibroblasts depending upon location of the injury in the lobule.<sup>2,7</sup> There are increasing data demonstrating an intimate cross-talk between LPC and  $\alpha$ SMA-positive myofibroblasts<sup>3,8-11</sup> and several studies in rodent models and human diseases have pointed out a strong relationship between severity of fibrosis and intensity of the ductular reaction.<sup>12-15</sup> Interactions between LPC and sinusoidal HSC or portal fibroblasts are poorly understood but their activation could occur independently, successively or in tandem through similar stimuli.<sup>16</sup> First, it can be considered that secretion of profibrogenic cytokines and growth factors by LPC could participate to portal fibrosis by inducing HSC or portal fibroblast activation,<sup>17,18</sup> but this implication of LPC in fibrosis has not been clearly shown *in vivo*. On the opposite, activation of HSC or portal fibroblasts into myofibroblasts producing extracellular matrix and growth factors, precedes LPC expansion and differentiation in periportal regions along a porto-venous axis.<sup>6,11</sup> Recently, it has been shown that inhibition of HSC activation greatly diminished LPC expansion.<sup>19</sup> Therefore, HSC or portal fibroblast activation seems a pre-requisite for LPC expansion, as already demonstrated in other stem cell niches.<sup>20</sup> Additionally, myofibroblast-LPC cross-talk could indirectly enhance fibrogenesis by recruiting cells of innate immune response, such as leukocytes required for wound healing.<sup>21</sup> Among the large variety of

factors secreted by myofibroblasts, transforming growth factor- $\beta$  (TGF $\beta$ ), the most potent fibrogenic cytokine, is also a well established mediator of epithelial-mesenchymal transition (EMT), which contributes to fibrosis following injury in several organs including the liver.<sup>22-26</sup>

To investigate the fibrogenic potential of LPC, we established a new model in the rat in which persistent LPC expansion induced by a chronic 2-acetylaminofluorene (AAF) treatment was combined to the well-established model of liver fibrosis using chronic carbon tetrachloride (CCl<sub>4</sub>) injection.<sup>1</sup> Metabolism of CCl<sub>4</sub> into highly reactive CCl<sub>3</sub> radicals by cytochrome P450; is responsible for centrilobular hepatocellular necrosis which triggers matrix deposition starting around the central veins, with gradual formation of septa bridging neighboring central veins, without any ductular reaction.<sup>25</sup> In our model, administration of AAF prior to and during CCl<sub>4</sub>-treatment blocks the proliferative hepatocyte response caused by CCl<sub>4</sub>-induced necrosis<sup>27</sup> and leads to the emergence of an alternate regenerative pathway with expansion of LPC in periportal regions as commonly reported in human fibrosis of various etiologies.<sup>12-14,28</sup> Using this new model, we investigated the involvement of LPC activation in fibrosis development by comparing the fibrogenic response in rats treated with a combination of CCl<sub>4</sub> and AAF to that obtained in animals treated with either CCl<sub>4</sub> or AAF alone. We also investigated whether LPC may directly participate to fibrogenesis and serve as a source of myofibroblasts through EMT as reported for hepatocytes and biliary cells.<sup>22-26</sup>

## **Materials and Methods**

### **Animals and experimental design**

200g male Sprague Dawley rats (Janvier Animal Center) received intraperitoneal injection of CCl<sub>4</sub> (Sigma-Aldrich) diluted 1/1 in olive oil twice a week in combination with 2-acetylaminofluorene (0.02% AAF in pellet form, Genestyl) treatment (AAF/CCl<sub>4</sub> group, n=27) for 6 weeks. AAF was given five days before the first CCl<sub>4</sub> injection. In a preliminary study, a continuous AAF exposition in association with a commonly used CCl<sub>4</sub> dose (2ml/kg of body weight) was not well tolerated leading to a severe weight loss after 4 weeks of treatment and a high rate of animal mortality. For these reasons, we used 2ml/kg of body weight for the initial CCl<sub>4</sub> injection and half of this dose for subsequent injections (i.e., 1ml/kg body

weight). From the second week, the AAF treatment was discontinued 3 days a week (replaced by standard chow). Rats were sacrificed 2, 4 or 6 weeks after the first CCl<sub>4</sub> injection and 48 hours after the last CCl<sub>4</sub> injection and due to significant mortality in this group, 7 to 9 animals were analyzed per time point. Two other animal groups received either CCl<sub>4</sub> only (CCl<sub>4</sub> group, n=27) or AAF only (AAF group, n=13). . An additional group of untreated rats was used as a control and fed a standard rat chow *ad libitum* (control group, n=7). The livers were removed from animals under anaesthesia and processed as previously described.<sup>29</sup> Blood samples were collected to measure serum alanine aminotransferase (ALT) activity by using an Advia 1650 automate (Bayer Diasys). Animal manipulations were performed according to the recommendations of the French ethical committee and under the supervision of authorized investigators.

### **Caspase-3 activity.**

Liver lysates were prepared by homogenization in hypotonic buffer (50 mM HEPES pH 7.5, 100 mM NaCl, 1% NP40, 1mM EGTA pH8, 1 mM DTT, protease inhibitor cocktail (Roche)). Homogenates were centrifuged at 10 000 g. for 15 min, and extracted proteins (50 µg) were tested in duplicate experiments by measuring the proteolytic cleavage of Ac-DEVD-AFC fluorogenic substrate for caspase-3 (Biomol) on microplate reader TriStar LB 941 (Berthold) as previously described.<sup>30</sup>

### **Histopathological and immunohistochemical methods**

Liver injury and fibrosis were assessed on 4 µm-thick paraffin-embedded liver sections stained with hematoxylin and eosin (H&E) and picrosirius red, respectively. Immunohistochemistry was carried out on paraffin-embedded or 5 µm-thick frozen sections, as previously described.<sup>29</sup> Primary antibodies were mouse monoclonal anti-cytokeratin 19 (CK19) (1:150, Novocastra laboratories), anti-alpha-smooth muscle actin (αSMA) (1:1000, Sigma-Aldrich), anti-desmin (1:200, DakoCytomotion), anti-CD68 (1:150, Serotec) and rabbit polyclonal anti-collagen 1 (1:200, Serotec) or anti-TGFβ (1:50 Santa Cruz). Fluorescent labeling of CK19 and CD68 was achieved on 6 µm frozen sections using secondary goat anti-mouse IgG Alexa fluor 488 and 555 respectively (1:1000), after incubation with the Image-iT™FX signal enhancer to reduce the background (Invitrogen). Computer-assisted quantitation of the relative surface

stained by CD68 on liver section at magnification x100 was performed with ImageJ (NIH). Immunodetection of  $\alpha$ -SMA on paraffin-embedded sections used the streptavidin-alkaline phosphatase conjugate (Serotec) and the FastRed substrate systems (Dako). Double-staining experiments were performed on 6  $\mu$ m frozen sections. Immunofluorescence double staining of collagen1 and CK19 was revealed with the secondary goat anti-rabbit IgG Alexa fluor 555 and anti-mouse IgG Alexa fluor 488, and double staining of TGF $\beta$  and CK19 with the secondary goat anti-rabbit IgG Alexa fluor 488 and anti-mouse IgG Alexa fluor 555, respectively. When mouse primary antibodies directed against  $\alpha$ SMA or desmin were used, they were incubated alone and detected with goat anti-mouse IgG Alexa fluor 555. After a 20 minute step of permeabilization by 0.2% triton in PBS, sections were incubated with an anti-CK19 antibody directly labeled with mouse IgG Alexa fluor 488, using Zenon® labeling technology (Invitrogen).

### ***In situ* hybridization**

Complementary RNA probe specific for  $\alpha$ -fetoprotein (AFP) and TGF $\beta$  were synthesized using a digoxigenin RNA labeling kit (Roche Diagnostics). The cRNA AFP probes were obtained from a rat cDNA plasmid (gift of Dr JL. Danan) digested with XmaI (antisense) or SphI (sense) probe) and transcribed from the SP6 or T7 promoters, respectively. TGF $\beta$  probes were transcribed from a cDNA fragment obtained by RT-PCR from rat liver at day 9 in the AAF/partial hepatectomy model using forward 5'-TACGTCAGACATTCGGGAAGCAGT-3' and reverse 5'-TG TACTGTGTGTCCAGGCTCCAAA-3' primers which map to positions 553-576 and 1143-1131 of the rat TGF $\beta$  sequence (GI: 148747597) and subcloned into pCR4-TOPO-plasmid. The cRNA TGF $\beta$  probes were transcribed from T7 and T3 promoters of the plasmid digested with SpeI (antisense) or NotI (sense) and labeling, hybridization and revelation procedures were performed in paraffin sections as previously described.<sup>31</sup> Detection of AFP or TGF $\beta$  mRNA in consecutive liver sections stained with immunofluorescent anti-CK19 as describe above, were realized with a standard *in situ* hybridization protocol on frozen serial sections cut at 5 $\mu$ m thickness (Supplemental materials).

## Quantitative real-time PCR

Total RNA was isolated from frozen hepatic tissue using the RNeasy mini kit (Qiagen). Two µg were reverse-transcribed from random hexamers using a first-strand synthesis kit (Fermentas Life Sciences) and specific cDNA amplifications were performed as previously described<sup>29</sup> using primers listed in Table 1. Relative quantification of gene expression was performed using the  $2^{-\Delta\Delta CT}$  method and ribosomal 18S RNA normalization and results were expressed as fold induction over values obtained from control animals.

## Liver collagen content

Hydroxyproline assay was performed as previously described,<sup>32</sup> using small fragments of different lobes that were pooled, lyophilized and hydrolyzed in 6N HCl at 110°C overnight. Hepatic hydroxyproline content was spectrophotometrically measured using freshly prepared Ehrlich's reagent and results were expressed as µg/mg of tissue (dry weight).

**Statistical analysis :** Liver weight, mRNA and protein analysis (ALT, caspase-3, hydroxyproline) were determined in all animals in duplicate experiments and values are mean  $\pm$  SEM of 4-9 separate rats from each group and time point Two-way ANOVA was employed to assess the effect of each treatment over the weeks using Bonferroni post-test. The student's *t*-test was used to compare the differences between 2 groups. Statistical analyses were performed with PRISM (GraphPad) and *P*-value of less than or equal to 0.05 indicated a significant difference between groups (\* *P*<0.05, \*\* *P*<0.01 and \*\*\* *P*<0,001).

## Results

### Liver injury

CCl<sub>4</sub> treatment induced hepatocellular necrosis revealed by a gradually increase of serum ALT activity which reached their maximal values (238 $\pm$ 33 U/L) at week 6 in group CCl<sub>4</sub> (Figure 1A). CCl<sub>4</sub> treatment also provoked hepatic apoptosis as revealed by measurement of active caspase-3 in liver extracts (Figure 1A). No significant differences in necrosis and apoptosis were observed between the CCl<sub>4</sub> and AAF/ CCl<sub>4</sub>

animals by two-way ANOVA, indicating similar liver injury in both groups. Interestingly, AAF treated animals exhibited low ALT activities but values were significantly higher ( $52 \pm 8$  U/L;  $P < 0.05$ ) than control rats ( $37 \pm 5$  U/L). In contrast, AAF treatment produced the highest caspase-3 activity in all liver extracts tested, indicating that chronic AAF exposure alone induced marked hepatic apoptosis associated with a moderate hepatocellular necrosis.

After 6 weeks of treatment, animals from AAF/CCl<sub>4</sub> group had a body weight ( $262 \pm 20$  g) significantly ( $P < 0,001$ ) lower than in groups CCl<sub>4</sub> and AAF ( $370 \pm 28$  g and  $367 \pm 16$  g respectively). At the end of the treatment, the ratio of the liver weight to the body weight was increased in both groups of animals treated by CCl<sub>4</sub> as compared to untreated rats and induction in the AAF/ CCl<sub>4</sub> group was significantly higher than in CCl<sub>4</sub> group (Figure 1B).

Livers from group CCl<sub>4</sub> exhibited gradual hepatic parenchymal alterations in centrilobular areas with the length of the treatment (Figure 1C), in accordance with increased serum ALT. After 2 weeks of CCl<sub>4</sub> treatment, focal necrosis and steatotic hepatocytes were seen around the central veins (data not shown). Two weeks later, livers showed mild to moderate steatosis, often associated with inflammatory cell accumulation and bands of damaged tissue connecting central veins of adjacent lobules. After 6 weeks, the hepatic lobular structure was disorganized with moderate hepatocellular steatosis and ballooning in close proximity to inflammatory cells, leading in some cases to complete interconnection between central veins and thus dividing the parenchyma into pseudo-lobules centered by a portal tract. In the AAF/CCl<sub>4</sub> group after 2 weeks of treatment, hepatic centrilobular injury was similar to that observed in animals treated with CCl<sub>4</sub> alone, except for an expansion of basophilic cells with a high nuclear to cytoplasmic ratio detected in periportal areas (data not shown). After 4 weeks, basophilic cell infiltration extended more deeply into the lobule of AAF/CCl<sub>4</sub>-treated rats and formed porto-portal and porto-central bridges. Two weeks later, large areas of basophilic cells delineated multiple nodules in the liver, and hepatic steatosis was localized around these connecting areas. Unexpectedly in the AAF group, we also observed periportal expansion of basophilic cells with small ovoid nuclei, progressively linking adjacent portal areas after 6 weeks of treatment, although there was neither steatosis nor centrilobular necrosis (Figure 1C).

### **Liver precursor cell expansion**

In groups AAF and AAF/CCl<sub>4</sub> after 2 weeks of treatment, small basophilic cells arising from portal areas expressed cytokeratin 19 (CK19), a liver precursor cell marker (data not shown). In these two groups, CK19-positive cells increased in number with time and expanded inside the lobule, where they formed duct-like structures (Figure 2A). After 6 weeks in both groups, there was an extensive arborization of CK19-positive cells, which extended across the liver lobule, forming bridges between portal tracts. In addition, in group AAF/CCl<sub>4</sub>, expansion of CK19-positive cells connected portal and centrilobular areas, dividing the parenchyma into smaller pseudo-lobules. As expected, such an accumulation of CK19-positive cells was not detected in CCl<sub>4</sub>-treated rats, where labeling was restricted to bile duct-cells in portal tracts (Figure 2A), as in normal liver (data not shown). These results were confirmed by real-time PCR analysis, which revealed an increase of hepatic CK19 mRNA expression only in AAF and AAF/CCl<sub>4</sub> groups, peaking at 93-fold over the basal level at week 4 and 6 in AAF/CCl<sub>4</sub>-treated rats (Figure 2B). No significant difference was observed between the AAF and AAF/CCl<sub>4</sub> groups, suggesting that CCl<sub>4</sub> treatment did not contribute to CK19-positive cell expansion induced by AAF. These latter cells organized in ductular structures also expressed AFP mRNA detected by *in situ* hybridization, confirming their precursor phenotype (Figure 2C). Similar results were obtained on consecutive liver section stained with immunofluorescent antibody against CK19 (red) and *in situ* hybridization for AFP mRNA (Supplementary Figure S1). In summary, chronic AAF treatment activated the hepatic stem cell compartment leading to LPC proliferation, which was similar in AAF and AAF/CCl<sub>4</sub> groups. Porto-central connections formed by proliferating LPC and only observed in the AAF/CCl<sub>4</sub> group, seemed to be related to CCl<sub>4</sub>-induced lesions.

### **Liver fibrosis**

As expected, rats treated with chronic CCl<sub>4</sub> injection displayed progressive liver fibrosis detected by picrosirius red-staining (Figure 3A). At week 2 in group CCl<sub>4</sub>, fibrosis was first demonstrated around centrilobular venules, with deposition of thin collagen fibers in necrotic and steatotic areas (data not

shown). At week 4, we observed gradual formation of fibrous septa interconnecting centrilobular areas, without disorganization of the lobular architecture. After 6 weeks, multiple centro-central fibrotic septa incompletely compassed and divided hepatic lobules. Unexpectedly, in AAF-treated animals after 4 weeks, thin collagen deposition arose from portal tracts and progressed into the lobule in close proximity to the LPC expansion at week 6 (Figure 2A), suggesting that the faint picosirius red-signal might correspond to type 4 collagen accumulation,<sup>33</sup> a major component of basement membrane associated to LPC activation.<sup>2</sup> Immunofluorescence detection of collagen 1 revealed an accumulation of this major component of liver fibrosis in group CCl<sub>4</sub> (Figure 3B), whereas a faint fluorescent signal was detected in group AAF. In accordance with these observations, real-time PCR analysis (Figure 3C) demonstrated an induction of hepatic mRNA expression of collagen type 1 and 3 in group CCl<sub>4</sub> and collagen 4 in group AAF. Thus, the 2-times induction of the hydroxyproline content (Figure 3D) can be accounted by the accumulation of fibrotic collagens in group CCl<sub>4</sub> and the extension of basement membrane associated with LPC expansion in group AAF.

In animals treated by a combination of AAF and CCl<sub>4</sub>, disease progression and the fibrotic pattern corresponded to the responses above described in both CCl<sub>4</sub> and AAF groups (Figure 3A). After 4 weeks, picosirius red-staining revealed thin fibrous septa from the portal tracts interconnected with larger fibrous scars from central veins, leading to porto-portal and porto-central fibrosis. After 6 weeks, fibrosis was more extensive, delineating multiple micronodules and forming complete cirrhosis in all rats from the AAF/CCl<sub>4</sub> group. PCR analysis (Figure 3C) showed significantly increased hepatic mRNA expression of collagen type 1 and 3, by comparison with that was noted in animals treated only by CCl<sub>4</sub> (ANOVA  $p < 0.05$ ). There was also an induction of hepatic collagen type 4, similar to that observed in group AAF. An increase of the hydroxyproline content in AAF/CCl<sub>4</sub> group (Figure 3D) up to 7 fold over basal level at week 6, and significantly higher than in CCl<sub>4</sub> and AAF groups (ANOVA  $p < 0.001$ ), was in accordance with increased fibrosis demonstrated by picosirius red-staining (Figure 3A). Thus, in group AAF/CCl<sub>4</sub>, active deposition of basement membrane components during LPC expansion also takes a part in the fibrogenic process, indicating that AAF, while stimulating an expansion of LPC, exacerbates CCl<sub>4</sub>-induced liver fibrosis.

## Liver inflammation

CCl<sub>4</sub> administration induces an inflammatory response, and macrophages play a critical role in myofibroblastic transformation of HSC and hepatic fibrogenesis.<sup>1</sup> The amount of liver macrophages, including Kupffer cells and recruited monocytes, was assessed by detection of the pan-macrophage CD68 antigen (Figure 4A). Normal liver displayed a homogenous lobular distribution of CD68-positive cells in accordance with Kupffer cell localization within sinusoids, and CD68 staining covered  $2.1 \pm 0.5$  % of the liver section as estimated by computer-assisted spot detection method (data not shown). In group CCl<sub>4</sub> after 4 weeks, small foci of CD68-positive cells accumulated in centro-central septa (Figure 4A), and increased in number with the duration of CCl<sub>4</sub> treatment, covering up to 6.3% of the liver section at week 6 (Figure 4B). In animals treated with AAF alone, the increase in CD68-labelled cells did not significantly differ from that noticed in group CCl<sub>4</sub> (Figure 4B), but most positive cells were regularly distributed all over liver lobules (Figure 4A), as noted for CD68-stained Kupffer cells in normal liver. In group AAF/CCl<sub>4</sub>, a majority of CD68-positive cells accumulated in the bridging septa above described (Figure 2A). Although extensive fibrosis was observed in AAF/CCl<sub>4</sub> group, the area of the CD68-stained liver tissue was not significantly different from that measured in the group CCl<sub>4</sub> (Figure 4B).

During liver injury, activated macrophages secrete numerous cytokines, including TNF $\alpha$ , which are mitogenic for hepatocytes<sup>34</sup> as well as for LPC.<sup>35,36</sup> In CCl<sub>4</sub>-treated rats, real-time PCR revealed a gradual but limited (less than 4 fold) induction of tumor necrosis factor- $\alpha$  (TNF $\alpha$ ) mRNA (Figure 4C) to a level which was not statistically different in AAF and AAF/CCl<sub>4</sub> groups. Even more, chemokine C-C motif receptor 2 (CCR2) mRNA, which is expressed only in recruited monocytes and some T lymphocytes,<sup>37</sup> was not different in the 3 groups (Figure 4D). The low and similar grade of inflammation in the three groups contrasts with the strong difference in fibrosis extension, suggesting that, in our experimental conditions, inflammation had not a major role in the fibrogenic process.

## Fibrogenic liver cells

In chronic liver diseases, portal fibroblasts and activated HSC exhibit phenotypic features of myofibroblasts, namely expression of  $\alpha$ SMA and extracellular matrix (ECM) proteins.<sup>1</sup> After 2 and 4 weeks of CCl<sub>4</sub> treatment, immunohistochemical staining of  $\alpha$ SMA revealed only a vascular labeling in group CCl<sub>4</sub> (Figure 5A), also detected in control livers (data not shown). At week 6,  $\alpha$ SMA-positive cells were observed in active fibrotic areas of only 3 treated animals out of 6 analyzed (Figure 5A). In contrast, in the AAF/CCl<sub>4</sub>-treated animals, numerous  $\alpha$ SMA-positive cells were seen around portal areas as early as 2 weeks after starting the treatment (Figure 5A and 5B). The  $\alpha$ SMA labeling was also observed in fibrous septa around centrilobular areas at week 4 and in perinodular fibrosis from cirrhotic rats at week 6 (Figure 5A and 5B). In the AAF group, whatever the time of treatment,  $\alpha$ SMA-staining was restricted to vessels as in normal liver and did not reveal any activated HSC in the areas of ductular reaction (Figure 5A). Immunofluorescence detection of  $\alpha$ SMA in frozen liver sections which provides a higher sensitivity as compared to immunodetection on paraffin sections, confirmed the lack of  $\alpha$ SMA-positive cells in the ductular reaction from group AAF and the presence of few activated HSC in fibrous septa in liver from group CCl<sub>4</sub> after 6 weeks of treatment (Figure 6A). Immunofluorescence detection of desmin, a hallmark of quiescent and activated HSC, showed an accumulation of positive cells in group AAF, closely associated to LPC expansion extending from periportal areas (Figure 6A). In group CCl<sub>4</sub>, desmin staining was detected in centrilobular injured areas and in centro-central fibrous septa. Thus, under our experimental setting (1ml/kg of CCl<sub>4</sub>), the paucity of  $\alpha$ SMA staining reflected minor myofibroblastic activation in agreement with moderate fibrosis. In summary, HSC transactivation was clearly shown only in liver from AAF/CCl<sub>4</sub>-treated animals, first in close proximity of LPC arising from portal areas, and then in bridging fibrosis, demonstrating that combination of CCl<sub>4</sub> and AAF was necessary to obtain  $\alpha$ SMA-positive myofibroblasts, which could account for the high degree of fibrosis in this group.

Transforming growth factor- $\beta$  (TGF $\beta$ ) is the major fibrogenic cytokine mainly produced by  $\alpha$ SMA-positive myofibroblasts,<sup>1,8</sup> and its expression coincides with LPC expansion during liver regeneration after AAF/partial hepatectomy in rats.<sup>17</sup> Real-time PCR analysis demonstrated that hepatic mRNA expression of this profibrogenic factor was significantly higher in AAF/CCl<sub>4</sub> group ( $p < 0.05$ ) than in the group which received CCl<sub>4</sub> alone (Figure 6B), in accordance with fibrosis extension. Unexpectedly,

TGF $\beta$  mRNA induction was higher in AAF than in CCl<sub>4</sub> group ( $p < 0.001$ ), notably after 2 and 4 weeks of treatment corresponding to the early stages of LPC activation. An increased TGF $\beta$  expression in both groups treated with AAF suggests that LPC are themselves a source of TGF $\beta$ , a result that has already been reported.<sup>4,38</sup> *In situ* hybridization studies were performed to identify more precisely the TGF $\beta$ -producing cells (Figure 6C). In rats treated with AAF alone for 6 weeks, numerous positive-cells for TGF $\beta$  mRNA expression were arranged as duct-like structures that deeply invaded the liver from portal areas. In this group without  $\alpha$ SMA-positive myofibroblasts (Figure 6A), TGF $\beta$  expression was noted in cells previously identified as LPC by CK19 staining (Figure 2A) and AFP expression (Figure 2C). In cirrhotic liver of AAF/CCl<sub>4</sub>-treated animals, TGF $\beta$  mRNA expression was detected in perinodular septa, within cells of the ductular reaction (Figure 6C); however, it cannot be excluded that part of the signal could also be attributed to  $\alpha$ SMA-positive myofibroblasts in close contact with LPC (Figure 5 and 6A). These results fit with the induction of TGF $\beta$  mRNA expression (Figure 6B) and the number of activated HSC and/or LPC that emerge in the liver after each treatment. Thus, the 5-fold induction of TGF $\beta$  mRNA after 6 weeks of treatment in the CCl<sub>4</sub> and AAF groups can be accounted by expression in HSC and LPC, respectively. The further induction up to 13 times in group AAF/CCl<sub>4</sub> can be related to TGF $\beta$  expression in both LPC and HSC, as a consequence of AAF-induced LPC expansion and CCl<sub>4</sub>-induced myofibroblastic activation; all these data reveal contribution of LPC to the development of liver fibrosis. To get better insight into TGF $\beta$  expression by LPC, we performed double-immunofluorescent detection of CK19 (red) and TGF $\beta$  (green) in liver sections from AAF/CCl<sub>4</sub>-treated rats. By confocal analysis, there was a yellow signal in merged analysis, revealing TGF $\beta$  staining in CK19-positive cells forming ductular structures (Figure 6D). This result was also confirmed on consecutive liver frozen sections labelled with fluorescent CK19 and *in situ* hybridization for TGF $\beta$  mRNA (Supplementary Figure S2). Indeed, we noted a clear superimposition of TGF $\beta$  and CK19 signals in serial sections, predominantly in the portal ductular reaction and in septa expanding into the lobules, both areas containing a large population of LPC in AAF-treated animals. DAPI labeling also revealed that TGF $\beta$  mRNA was largely confined to small

cells with ovoid nuclei, characteristic of LPC. Altogether, these results might strongly indicate that TGF $\beta$  was expressed by LPC.

### **Epithelial-mesenchymal transition of LPC**

To determine whether LPC undergo an epithelial-to-mesenchymal transition (EMT) in cirrhotic liver, we studied these CK19-positive cells for the expression of mesenchymal markers in AAF/CCl<sub>4</sub> group after 6 weeks of treatment. Double immunofluorescent experiments did not show any expression of  $\alpha$ SMA in CK19-positive LPC (no merging signals), neither in the ductular reaction arising in portal areas nor in fibrous septa (Figure 7A). Thus, the  $\alpha$ SMA-positive signal found in close contact of LPC corresponded to labeling of myofibroblastic HSC already described in the ductular reaction.<sup>3,11,15,39</sup> Desmin staining, which revealed HSC in contact with LPC, extended beyond  $\alpha$ SMA-labeled cells (Figure 7A), indicating that HSC detected in the ductular reaction are not fully activated into myofibroblastic cells. These results were confirmed by confocal analysis, which clearly showed the absence of  $\alpha$ SMA and desmin localization in CK19-labeled cells (Figure 7B). Additionally, expression of the fibroblast specific protein FSP1, which was also revealed around CK19-positive LPC (Figure 7A), did not co-stain in the same cells. Lack of colocalization of CK19 and collagen 1 (Figure 7A) suggests that the primary cells responsible for liver fibrogenesis are not LPC but activated HSC surrounding these cells. Therefore, we did not obtain any evidence showing that LPC might undergo EMT in AAF/CCl<sub>4</sub>-treated rats.

### **Discussion**

Hepatic fibrosis is the liver response to chronic liver injury. It is characterized by excessive matrix deposition and accumulation of LPC, which are usually initiated in periportal areas, whatever is the location of the damage in the lobule.<sup>1,13,14</sup> Classical models of fibrosis in rodents are based on chronic CCl<sub>4</sub> intoxication leading to hepatocyte necrosis and matrix accumulation, which appeared initially around the central veins, without any LPC proliferation.<sup>40</sup> AAF administration associated with single CCl<sub>4</sub> injection or partial hepatectomy is a classical experimental model to study LPC-dependent regeneration in rat.<sup>27</sup> In this study, we developed a new experimental model, which recapitulates the

events commonly observed in human fibrosis and is suitable to investigate the role of LPC in fibrogenesis. Indeed, the severity of liver fibrosis has been correlated to LPC expansion in human<sup>12-14,28</sup> and recently, unexpected activation of LPC compartment in *Egr1*<sup>-/-</sup> mice enhanced hepatic fibrosis after chronic CCl<sub>4</sub> exposure.<sup>41</sup> To achieve that goal, we combined an AAF treatment, known to induce regeneration from LPC,<sup>2,27</sup> with repeated CCl<sub>4</sub> injections, known to induce liver fibrosis in rodents. Combined AAF and CCl<sub>4</sub> treatment led to extensive liver fibrosis and cirrhosis with marked LPC expansion, whereas CCl<sub>4</sub> intoxication alone caused moderate fibrosis without expansion of LPC compartment. Unexpectedly, chronic and discontinuous AAF treatment by itself induced also an LPC expansion in absence of an external mitogenic stimulus. Actually, low AAF doses generated low toxicity as revealed by slight induction of ALAT, but liver injury was accompanied by an increase of apoptosis. This is in line with the proposal that AAF metabolites are able to uncouple mitochondrial respiratory chain and open the permeability pore leading to apoptosis.<sup>42</sup> As a consequence, injured hepatocytes eliminated by apoptosis might provide a sufficient signal to stimulate the LPC compartment while normal hepatocytes cannot proliferate due to AAF toxicity.

In all AAF/CCl<sub>4</sub>-treated rats, accumulation of LPC in fibrous septa was associated with enhanced activation of desmin-positive HSC and expression of profibrotic genes such as collagen 1 and 3, leading to cirrhosis. As recently reported,<sup>11</sup>  $\alpha$ SMA-positive cells were first detected in close association with LPC expansion in the portal region of the lobule at week 2. Activated HSC were observed later in necrotic centrilobular areas and in porto-central bridging fibrosis at week 6. In contrast, very few  $\alpha$ SMA-positive cells were detected in the liver of animals treated with CCl<sub>4</sub> only, probably because of the low dose of CCl<sub>4</sub> used in our experimental conditions, which represented only 50% of the amount generally used in fibrogenic protocols. Since paracrine and autocrine secretion of TGF $\beta$  is the main factor involved in matrix deposition by activated HSC,<sup>8</sup> reduced fibrosis in liver from CCl<sub>4</sub>-treated rats is in accordance with low level of TGF $\beta$  mRNA. Resident and recruited macrophages also play a critical role in myofibroblastic activation of HSC, notably by releasing factors including TGF $\beta$ .<sup>1</sup> However, the increased fibrogenic process in AAF/CCl<sub>4</sub>-treated rats did not essentially depend on the inflammatory response, which remained moderate in our experimental setting and similar in both CCl<sub>4</sub> and AAF/CCl<sub>4</sub> groups, as

assessed by CD68 labeling, TNF $\alpha$  and CCR2 mRNA levels. To investigate the underlying role of LPC on fibrosis, it was important to exclude a distinct effect in liver damage of combined AAF/CCl<sub>4</sub> treatment from CCl<sub>4</sub> alone. A similar level of liver injury was achieved in both groups, as shown by similar serum ALT and similar apoptosis in liver extracts at any experimental time point. This probably excludes additional AAF-induced toxicity as a complicating factor in AAF/CCl<sub>4</sub>-treated animals. Thus, defective HSC activation into  $\alpha$ SMA-positive cells and reduced fibrosis in CCl<sub>4</sub>-treated rats seemed to be related to the lack of LPC compartment expansion.

Activation of LPC is a complex process that is not elucidated yet. It involves secretion of cytokines such as TNF $\alpha$  that activates the entry of quiescent stem cell in the cell cycle in a context where liver regeneration from hepatocytes is severely impaired as reported in AAF/CCl<sub>4</sub> treated rats.<sup>36</sup> Other cytokines produced by immune cells in response to liver injury such as interferon- $\gamma$  have mitogenic effects on LPC and anti-proliferative effects on hepatocytes.<sup>43</sup> Interestingly, hedgehog (Hh) ligands released from dying hepatocytes can promote LPC expansion and the resistance of LPC to the antiproliferative response of TGF $\beta$ . They are probably other players of the LPC response in injured liver and by favouring activation of HSC or portal fibroblasts into myofibroblasts,<sup>44-46</sup> may also promote cirrhosis in AAF/CCl<sub>4</sub> group. Numerous studies have reported paracrine interactions between LPC and HSC or portal fibroblasts located in close proximity.<sup>2,11,14,15,47,48</sup> Activated HSC<sup>18,49</sup> and portal fibroblasts<sup>45</sup> are a major source of growth factors for LPC and recent data established that myofibroblasts are required for LPC response<sup>11,19</sup> and are a component of the LPC niche.<sup>20</sup> Conversely, it has not been clearly shown whether LPC could cause HSC or portal fibroblast activation. The  $\alpha$ SMA staining, the most widely used technique that reveals myofibroblasts, could not distinguish in our study between both types of cells. In the present study, we demonstrated that LPC express TGF $\beta$ , the most potent activator of quiescent HSC<sup>8</sup> and portal fibroblasts<sup>50</sup> into myofibroblasts, therefore contributing to hepatic fibrogenesis. The fact that TGF $\beta$  was also detected in LPC from rats treated with AAF alone in the absence of  $\alpha$ SMA-positive cells close to LPC, points out that LPC and TGF $\beta$  alone are not sufficient to induce activation of HSC or of portal fibroblasts. In the group AAF, we observed an enhanced hepatic expression of collagen 4 and an accumulation of laminin (data not shown), two components of the

basement membrane secreted by quiescent HSC in contact with LPC,<sup>3,20</sup> which may account for the faint picosirius red labeling around portal areas. In summary, these data suggest that LPC alone are not fibrogenic when there is no hepatocellular damage, and they emphasize the need of CCl<sub>4</sub>-induced injury to promote HSC activation and subsequent fibrosis. In other words, in addition to TGF $\beta$  secreted by LPC, the release of numerous factors from dying hepatocytes seems necessary to trigger the further myofibroblastic activation of HSC and the subsequent fibrogenic response.

The ability of LPC to transform into myofibroblasts through EMT is an interesting issue.<sup>51-53</sup> The role of EMT in fibrosis was established in lung and kidney and, in the liver, transition of hepatocytes, biliary cells and HSC has also been already reported.<sup>22-26</sup> TGF $\beta$ , which we found secreted by LPC, is a well-known EMT inducer<sup>22,23,25</sup> that could trigger LPC transition by an autocrine/paracrine pathway and provide a new potential mechanism of fibrosis. However, we could not demonstrate the expression of mesenchymal markers (i.e.,  $\alpha$ SMA, desmin and FSP1) in CK19-positive LPC cells from AAF/CCl<sub>4</sub>-treated rats *in vivo*. Transition of LPC organized in ductular structures into isolated myofibroblasts could be difficult to identify by colocalization of epithelial and mesenchymal markers, particularly if the loss of epithelial characteristics occurs early during EMT process. For these reasons, proof of LPC undergoing EMT *in vivo* needs a genetic fate mapping approach to track the fate of LPC during liver injury. Nevertheless, transition of LPC to myofibroblasts after treatment with TGF $\beta$  has indeed been previously obtained *in vitro*, using LPC isolated from rats fed a choline-deficient diet supplemented with ethionine.<sup>53</sup> In a search of the capability of LPC to undergo EMT into HSC, we cultured human HepaRG liver progenitor cells<sup>54</sup> and followed their epithelial and fibroblastic phenotypic characteristics in response to TGF $\beta$ . HepaRG underwent a phenotypic change from epithelial to mesenchymal-like cells *in vitro* on the basis of an increased expression of snail,  $\alpha$ SMA and collagens and a paralleled decrease of E-cadherin (unpublished data) as observed by Wang *et al* on rat LPC.<sup>53</sup> Demonstration of EMT *in vivo* is at the heart of a controversy and some investigators consider that EMT observed *in vitro* could be an artefact of cell culture.<sup>55,56</sup> Although isolated and cultured LPC possess some mesenchymal markers of HSC, such as collagen 1 and 3<sup>53</sup> and  $\alpha$ SMA<sup>48,51</sup>, an elegant fate-mapping study using the LPC marker Foxl1 demonstrated that all Foxl1-expressing cells and their progeny did not acquire a mesenchymal phenotype

during LPC expansion *in vivo*.<sup>52</sup> These Foxl1-positive cells are surrounded by fibroblastic cells expressing elastin, desmin and  $\alpha$ SMA, which reveals a potential crosstalk between LPC and these fibrogenic cells. In accordance with these data, we show that LPC neither acquire a mesenchymal phenotype through EMT *in vivo* nor directly participate to excessive ECM deposition. It remains that CK19-negative cells expressing mesenchymal markers were detected in close proximity to LPC, confirming that LPC are accompanied by  $\alpha$ SMA-positive cells that derive from HSC or periportal fibroblasts.<sup>10,11,15</sup> Other evidence suggests that HSC could differentiate into LPC with an intermediate phenotype,<sup>51,57</sup> adding further complexity to the mechanisms by which HSC or LPC contribute to liver fibrogenesis. Nevertheless, mesenchymal to epithelial transition of HSC could not be demonstrated in liver fibrosis induced by bile duct ligation or CCl<sub>4</sub> administration.<sup>58</sup>

In summary, we show that LPC expansion aggravates liver fibrosis. This strong fibrogenic response does not appear to be the direct consequence of hepatocellular lesions or inflammatory response, but seems to be due to the accumulation of TGF $\beta$ -producing LPC, thus driving the myofibroblastic transformation of fibroblasts and/or HSC in injured liver. Fibrogenic properties of periportal LPC provide an explanation for the development of predominant periportal fibrosis, whatever is the primary location of hepatocellular damage, leading to porto-central fibrous septa progressing to cirrhosis.

## **Acknowledgement**

This work was supported by INSERM, University Paris-Est Creteil and Agence Nationale pour la Recherche (ANR-06-Physio-022-2). We are grateful for X. Decrouy from Platform for cell imaging (IMRB, Creteil) for technical support in confocal microscope.

## **Conflict of interest**

The authors declare no conflict of interest.

Supplementary information is available at Laboratory Investigation's website

## References

- 1 Ramadori G, Saile B. Portal tract fibrogenesis in the liver. *Lab Invest* 2004; 84(2):153-159.
- 2 Paku S, Schnur J, Nagy P, et al. Origin and structural evolution of the early proliferating oval cells in rat liver. *Am J Pathol* 2001; 158(4):1313-1323.
- 3 Paku S, Nagy P, Kopper L, et al. 2-acetylaminofluorene dose-dependent differentiation of rat oval cells into hepatocytes: confocal and electron microscopic studies. *Hepatology* 2004; 39(5):1353-1361.
- 4 Knight B, Matthews VB, Olynyk JK, et al. Jekyll and Hyde: evolving perspectives on the function and potential of the adult liver progenitor (oval) cell. *Bioessays* 2005; 27(11):1192-1202.
- 5 Sell S. Comparison of liver progenitor cells in human atypical ductular reactions with those seen in experimental models of liver injury. *Hepatology* 1998; 27(2):317-331.
- 6 Bird TG, Lorenzini S, Forbes SJ. Activation of stem cells in hepatic diseases. *Cell Tissue Res* 2008; 331(1):283-300.
- 7 Schotanus BA, van den Ingh TS, Penning LC, et al. Cross-species immunohistochemical investigation of the activation of the liver progenitor cell niche in different types of liver disease. *Liver Int* 2009; 29(8):1241-1252.
- 8 Friedman SL. Mechanisms of hepatic fibrogenesis. *Gastroenterology* 2008; 134(6):1655-1669.
- 9 Fausto N, Campbell JS, Riehle KJ. Liver regeneration. *Hepatology* 2006; 43(2 Suppl 1):S45-53.
- 10 Svegliati-Baroni G, De Minicis S, Marzioni M. Hepatic fibrogenesis in response to chronic liver injury: novel insights on the role of cell-to-cell interaction and transition. *Liver Int* 2008; 28(8):1052-1064.
- 11 Van Hul NK, Abarca-Quinones J, Sempoux C, et al. Relation between liver progenitor cell expansion and extracellular matrix deposition in a CDE-induced murine model of chronic liver injury. *Hepatology* 2009; 49(5):1625-1635.
- 12 Lowes KN, Brennan BA, Yeoh GC, et al. Oval cell numbers in human chronic liver diseases are directly related to disease severity. *Am J Pathol* 1999; 154(2):537-541.
- 13 Clouston AD, Powell EE, Walsh MJ, et al. Fibrosis correlates with a ductular reaction in hepatitis C: roles of impaired replication, progenitor cells and steatosis. *Hepatology* 2005; 41(4):809-818.

- 14 Richardson MM, Jonsson JR, Powell EE, et al. Progressive fibrosis in nonalcoholic steatohepatitis: association with altered regeneration and a ductular reaction. *Gastroenterology* 2007; 133(1):80-90.
- 15 Knight B, Akhurst B, Matthews VB, et al. Attenuated liver progenitor (oval) cell and fibrogenic responses to the choline deficient, ethionine supplemented diet in the BALB/c inbred strain of mice. *J Hepatol* 2007; 46(1):134-141.
- 16 Clouston AD, Jonsson JR, Powell EE. Hepatic progenitor cell-mediated regeneration and fibrosis: chicken or egg? *Hepatology* 2009; 49(5):1424-1426.
- 17 Pi L, Oh SH, Shupe T, et al. Role of connective tissue growth factor in oval cell response during liver regeneration after 2-AAF/PHx in rats. *Gastroenterology* 2005; 128(7):2077-2088.
- 18 Akhurst B, Matthews V, Husk K, et al. Differential lymphotoxin-beta and interferon gamma signaling during mouse liver regeneration induced by chronic and acute injury. *Hepatology* 2005; 41(2):327-335.
- 19 Pintilie DG, Shupe TD, Oh SH, et al. Hepatic stellate cells' involvement in progenitor-mediated liver regeneration. *Lab Invest* 2010.
- 20 Lorenzini S, Bird TG, Boulter L, et al. Characterisation of a stereotypical cellular and extracellular adult liver progenitor cell niche in rodents and diseased human liver. *Gut* 2010; 59(5):645-654.
- 21 Ruddell RG, Knight B, Tirnitz-Parker JE, et al. Lymphotoxin-beta receptor signaling regulates hepatic stellate cell function and wound healing in a murine model of chronic liver injury. *Hepatology* 2009; 49(1):227-239.
- 22 Kaimori A, Potter J, Kaimori JY, et al. Transforming growth factor-beta1 induces an epithelial-to-mesenchymal transition state in mouse hepatocytes in vitro. *J Biol Chem* 2007; 282(30):22089-22101.
- 23 Zeisberg M, Yang C, Martino M, et al. Fibroblasts derive from hepatocytes in liver fibrosis via epithelial to mesenchymal transition. *J Biol Chem* 2007; 282(32):23337-23347.
- 24 Robertson H, Kirby JA, Yip WW, et al. Biliary epithelial-mesenchymal transition in posttransplantation recurrence of primary biliary cirrhosis. *Hepatology* 2007; 45(4):977-981.

- 25 Rygiel KA, Robertson H, Marshall HL, et al. Epithelial-mesenchymal transition contributes to portal tract fibrogenesis during human chronic liver disease. *Lab Invest* 2008; 88(2):112-123.
- 26 Battaglia S, Benzoubir N, Nobilet S, et al. Liver cancer-derived hepatitis C virus core proteins shift TGF-Beta responses from tumor suppression to epithelial-mesenchymal transition. *PLoS ONE* 2009; 4(2):e4355.
- 27 Petersen BE, Zajac VF, Michalopoulos GK. Hepatic oval cell activation in response to injury following chemically induced periportal or pericentral damage in rats. *Hepatology* 1998; 27(4):1030-1038.
- 28 Roskams T, Yang SQ, Koteish A, et al. Oxidative stress and oval cell accumulation in mice and humans with alcoholic and nonalcoholic fatty liver disease. *Am J Pathol* 2003; 163(4):1301-1311.
- 29 Lafdil F, Chobert MN, Deveaux V, et al. Growth arrest-specific protein 6 deficiency impairs liver tissue repair after acute toxic hepatitis in mice. *J Hepatol* 2009; 51(1):55-66.
- 30 Lafdil F, Chobert MN, Couchie D, et al. Induction of Gas6 protein in CCl4-induced rat liver injury and anti-apoptotic effect on hepatic stellate cells. *Hepatology* 2006; 44(1):228-239.
- 31 Mavier P, Martin N, Couchie D, et al. Expression of stromal cell-derived factor-1 and of its receptor CXCR4 in liver regeneration from oval cells in rat. *Am J Pathol* 2004; 165(6):1969-1977.
- 32 Julien B, Grenard P, Teixeira-Clerc F, et al. Antifibrogenic role of the cannabinoid receptor CB2 in the liver. *Gastroenterology* 2005; 128(3):742-755.
- 33 Tullberg-Reinert H, Jundt G. In situ measurement of collagen synthesis by human bone cells with a sirius red-based colorimetric microassay: effects of transforming growth factor beta2 and ascorbic acid 2-phosphate. *Histochem Cell Biol* 1999; 112(4):271-276.
- 34 Fausto N, Laird AD, Webber EM. Liver regeneration. 2. Role of growth factors and cytokines in hepatic regeneration. *Faseb J* 1995; 9(15):1527-1536.
- 35 Knight B, Yeoh GC. TNF/LTalpha double knockout mice display abnormal inflammatory and regenerative responses to acute and chronic liver injury. *Cell Tissue Res* 2005; 319(1):61-70.
- 36 Knight B, Yeoh GC, Husk KL, et al. Impaired preneoplastic changes and liver tumor formation in tumor necrosis factor receptor type 1 knockout mice. *J Exp Med* 2000; 192(12):1809-1818.

- 37 Mitchell C, Couton D, Couty JP, et al. Dual role of CCR2 in the constitution and the resolution of liver fibrosis in mice. *Am J Pathol* 2009; 174(5):1766-1775.
- 38 Braun L, Mead JE, Panzica M, et al. Transforming growth factor beta mRNA increases during liver regeneration: a possible paracrine mechanism of growth regulation. *Proc Natl Acad Sci U S A* 1988; 85(5):1539-1543.
- 39 Pham Van T, Couchie D, Martin-Garcia N, et al. Expression of matrix metalloproteinase-2 and -9 and of tissue inhibitor of matrix metalloproteinase-1 in liver regeneration from oval cells in rat. *Matrix Biol* 2008; 27(8):674-681.
- 40 Zhao XY, Wang BE, Li XM, et al. Newly proposed fibrosis staging criterion for assessing carbon tetrachloride- and albumin complex-induced liver fibrosis in rodents. *Pathol Int* 2008; 58(9):580-588.
- 41 Pritchard MT, Nagy LE. Hepatic fibrosis is enhanced and accompanied by robust oval cell activation after chronic carbon tetrachloride administration to Egr-1-deficient mice. *Am J Pathol* 2010; 176(6):2743-2752.
- 42 Neumann HG. Aromatic amines in experimental cancer research: tissue-specific effects, an old problem and new solutions. *Crit Rev Toxicol* 2007; 37(3):211-236.
- 43 Viebahn CS, Yeoh GC. What fires prometheus? The link between inflammation and regeneration following chronic liver injury. *Int J Biochem Cell Biol* 2008; 40(5):855-873.
- 44 Nguyen LN, Furuya MH, Wolfraim LA, et al. Transforming growth factor-beta differentially regulates oval cell and hepatocyte proliferation. *Hepatology* 2007; 45(1):31-41.
- 45 Omenetti A, Yang L, Li YX, et al. Hedgehog-mediated mesenchymal-epithelial interactions modulate hepatic response to bile duct ligation. *Lab Invest* 2007; 87(5):499-514.
- 46 Jung Y, Witek RP, Syn WK, et al. Signals from dying hepatocytes trigger growth of liver progenitors. *Gut* 2010; 59(5):655-665.
- 47 Evarts RP, Nakatsukasa H, Marsden ER, et al. Cellular and molecular changes in the early stages of chemical hepatocarcinogenesis in the rat. *Cancer Res* 1990; 50(11):3439-3444.
- 48 Yovchev MI, Grozdanov PN, Zhou H, et al. Identification of adult hepatic progenitor cells capable of repopulating injured rat liver. *Hepatology* 2008; 47(2):636-647.

- 49 Knight B, Lim R, Yeoh GC, et al. Interferon-gamma exacerbates liver damage, the hepatic progenitor cell response and fibrosis in a mouse model of chronic liver injury. *J Hepatol* 2007; 47(6):826-833.
- 50 Li Z, Dranoff JA, Chan EP, et al. Transforming growth factor-beta and substrate stiffness regulate portal fibroblast activation in culture. *Hepatology* 2007; 46(4):1246-1256.
- 51 Sicklick JK, Choi SS, Bustamante M, et al. Evidence for epithelial-mesenchymal transitions in adult liver cells. *Am J Physiol Gastrointest Liver Physiol* 2006; 291(4):G575-583.
- 52 Sackett SD, Li Z, Hurtt R, et al. Foxl1 is a marker of bipotential hepatic progenitor cells in mice. *Hepatology* 2009; 49(3):920-929.
- 53 Wang P, Liu T, Cong M, et al. Expression of extracellular matrix genes in cultured hepatic oval cells: an origin of hepatic stellate cells through transforming growth factor beta? *Liver Int* 2009; 29(4):575-584.
- 54 Parent R, Marion MJ, Furio L, et al. Origin and characterization of a human bipotent liver progenitor cell line. *Gastroenterology* 2004; 126(4):1147-1156.
- 55 Taura K, Miura K, Iwaisako K, et al. Hepatocytes do not undergo epithelial-mesenchymal transition in liver fibrosis in mice. *Hepatology* 2010; 51(3):1027-1036.
- 56 Duffield JS. Epithelial to mesenchymal transition in injury of solid organs: fact or artifact? *Gastroenterology* 2010; 139(4):1081-1083, 1083 e1081-1085.
- 57 Yang L, Jung Y, Omenetti A, et al. Fate-mapping evidence that hepatic stellate cells are epithelial progenitors in adult mouse livers. *Stem Cells* 2008; 26(8):2104-2113.
- 58 Scholten D, Osterreicher CH, Scholten A, et al. Genetic labeling does not detect epithelial-to-mesenchymal transition of cholangiocytes in liver fibrosis in mice. *Gastroenterology* 2010; 139(3):987-998.

## Figure legends

**Figure 1** : Liver injury and histopathology. **A)** Serum ALAT activity was increased to a level which was similar in CCl<sub>4</sub> and AAF/CCl<sub>4</sub>-treated rats and significantly higher than in AAF-treated rats. Elevation of fluorometric caspase-3 activity was similar in rat liver treated either by CCl<sub>4</sub> or AAF/CCl<sub>4</sub> and was significantly higher in AAF-treated animals. **B)** The liver weight to body weight ratio was significantly increased in AAF/CCl<sub>4</sub>-treated rats after 6 weeks of treatment as compared to the other groups. # (P<0.05) denotes significant difference from control diet and \*\* (P<0.001) between AAF/CCl<sub>4</sub> and CCl<sub>4</sub>-treated animals. **C)** Representative H&E staining of liver sections after 4 (W4) and 6 weeks (W6) of treatment (original magnifications x40 and x400 as indicated) show steatosis and ballooned hepatocytes (arrows) in CCl<sub>4</sub>-treated animals (n=9) with formation of centro-central bridges dividing the hepatic parenchyma into lobules centered by portal tracts. In group AAF/CCl<sub>4</sub> (n=9), centrilobular injury was associated with expansion of basophilic cells extending from portal areas and leading to nodules. Proliferation of these cells with small ovoid nuclei in periportal areas was also observed in AAF-treated rats (n=4). PT denotes portal tracts.

**Figure 2** : LPC compartment activation. **A)** Representative immunofluorescent detection of CK19-positive cells in liver sections revealed an accumulation of LPC in rats treated with AAF (n=4) and AAF/CCl<sub>4</sub> (n=9), arising from portal areas at 4 weeks and expanding inside the lobule after 6 weeks of treatment (original magnification x200). Insets show higher magnification of CK19 labeling. Such an accumulation of LPC was not detected in CCl<sub>4</sub> group (n=9) where CK19 labeling was restricted to bile duct cells. **B)** Real-time PCR revealed an increase of CK19 mRNA expression only in AAF and AAF/CCl<sub>4</sub> groups. **C)** AFP mRNA detected by *in situ* hybridization (AFP AS probe) was restricted to cells of the ductular reaction in AAF and AAF/CCl<sub>4</sub>-treated animals. No specific signal was observed using AFP sense probe (original magnification x400). \* denotes portal tract. Images are representative of three independent experiments from three different rat liver sections.

**Figure 3 :** Liver fibrosis. **A)** Picrosirius red staining revealed progressive liver fibrosis induced by CCl<sub>4</sub> at week 4, with formation of centro-central fibrous septa at week 6. In AAF/CCl<sub>4</sub>-treated rats, marked fibrosis with porto-central bridging was observed at week 4, leading to cirrhosis at week 6. In portal areas of animals from AAF group, a faint picrosirius red staining was observed around LPC expansion. Original magnification x100. Images are representative of 4 (AAF) to 9 (CCl<sub>4</sub> or AAF/CCl<sub>4</sub>) liver sections. **B)** After 6 weeks, immunofluorescent collagen 1 detection revealed strong matrix deposition in perinodular areas from cirrhotic rats liver treated by AAF/CCl<sub>4</sub>. A lower collagen accumulation was detected in fibrous septa after CCl<sub>4</sub> administration, and a weak labeling was observed in the AAF-induced ductular reaction. Representative fluorescence photomicrographs of two experiments on liver sections from 3 rats in each group at magnification x200. **C)** Quantitative RT-PCR analysis showed a gradual induction of interstitial collagen type 1 and 3 mRNA enhanced in AAF/CCl<sub>4</sub>-treated rats as compared to CCl<sub>4</sub> treatment alone. Induction of collagen 4 mRNA was shown only in AAF and AAF/CCl<sub>4</sub> groups associated with LPC expansion. **D)** Total liver collagen content determined by hydroxyproline (OH-Pro) assay was higher in AAF/CCl<sub>4</sub>-treated rats.

**Figure 4 :** Macrophage recruitment and inflammation. **A)** CD68 immunofluorescent detection (original magnification x200) revealed positive cells all over liver parenchyma in AAF group, in fibrous septa after CCl<sub>4</sub> treatment and in the cirrhotic liver of AAF/CCl<sub>4</sub>-treated animals. Images are representative of 4 (AAF) to 6 (CCl<sub>4</sub> or AAF/CCl<sub>4</sub>) liver sections. \* denotes portal tracts. **B)** Quantification of CD68-positive cells in liver from animals did not reveal a significant difference in the number of hepatic macrophages in CCl<sub>4</sub> and AAF/CCl<sub>4</sub> groups after 4 or 6 weeks of treatment. Data are means ± SEM of separate analysis on two fields for each liver section from 4 (AAF) to 6 (CCl<sub>4</sub> or AAF/CCl<sub>4</sub>) separate rats. Quantitative RT-PCR did not demonstrate quantitative differences in **C)** TNF $\alpha$  or **D)** CCR2 mRNA expression, revealing that inflammatory response was similar in the 3 groups.

**Figure 5 :** HSC or portal fibroblast activation. **A)** Immunohistochemical detection of  $\alpha$ SMA-positive cells revealed few activated HSC delineating portal vessels after 6 weeks of CCl<sub>4</sub> administration alone. In

contrast, numerous positive cells were detected in AAF/CCl<sub>4</sub>-treated rats around portal areas at week 2, in fibrous septa at week 4 and in perinodular areas at week 6. No  $\alpha$ SMA-positive cell was observed in the ductular reaction in AAF group. Images are representative of 4 (AAF) to 9 (CCl<sub>4</sub> or AAF/CCl<sub>4</sub>) liver sections at original magnification x100. **B)** After 6 weeks of CCl<sub>4</sub> treatment, higher magnification (x400) clearly showed  $\alpha$ SMA-positive cells in centro-central fibrous septa containing marked collagen deposition revealed by picrosirius red staining. By contrast, in AAF/CCl<sub>4</sub>-treated rats, activation of HSC or portal fibroblasts was early detected at week 2, around the LPC arising in periportal areas faintly stained by picrosirius red. At week 6,  $\alpha$ SMA labeling was noted in bridging fibrous septa with large amount of collagen deposition.

**Figure 6 :** Detection of fibrogenic liver cells. **A)** Immunofluorescent detection of  $\alpha$ SMA and desmin after 6 weeks of treatment confirms activation of HSC into  $\alpha$ SMA-expressing myofibroblasts in cirrhotic liver of AAF/CCl<sub>4</sub>-treated rats. Very few  $\alpha$ SMA-positive HSC were noted in fibrous septa after CCl<sub>4</sub> administration alone. Lack of activated HSC was observed around the portal areas in the AAF-induced ductular reaction. Representative fluorescence photomicrographs of two experiments on liver sections from 2 rats in each group at original magnification x200. **B)** Quantitative RT-PCR analysis revealed an enhanced induction of TGF $\beta$  mRNA expression in AAF and AAF/CCl<sub>4</sub>-treated animals and **C)** TGF $\beta$  mRNA detection by *in situ* hybridization showed a strong positive signal in LPC in duct-like structures (inset contains sense probe labeling) in both groups (original magnification x400). **D)** Double-immunofluorescent detection of TGF $\beta$  (green) and CK19 (red) proteins in liver sections from AAF/CCl<sub>4</sub>-treated rats, revealed TGF $\beta$ -expressing LPC in merged imaged by confocal analysis. Images are representative of two independent experiments from three different rats in each group.

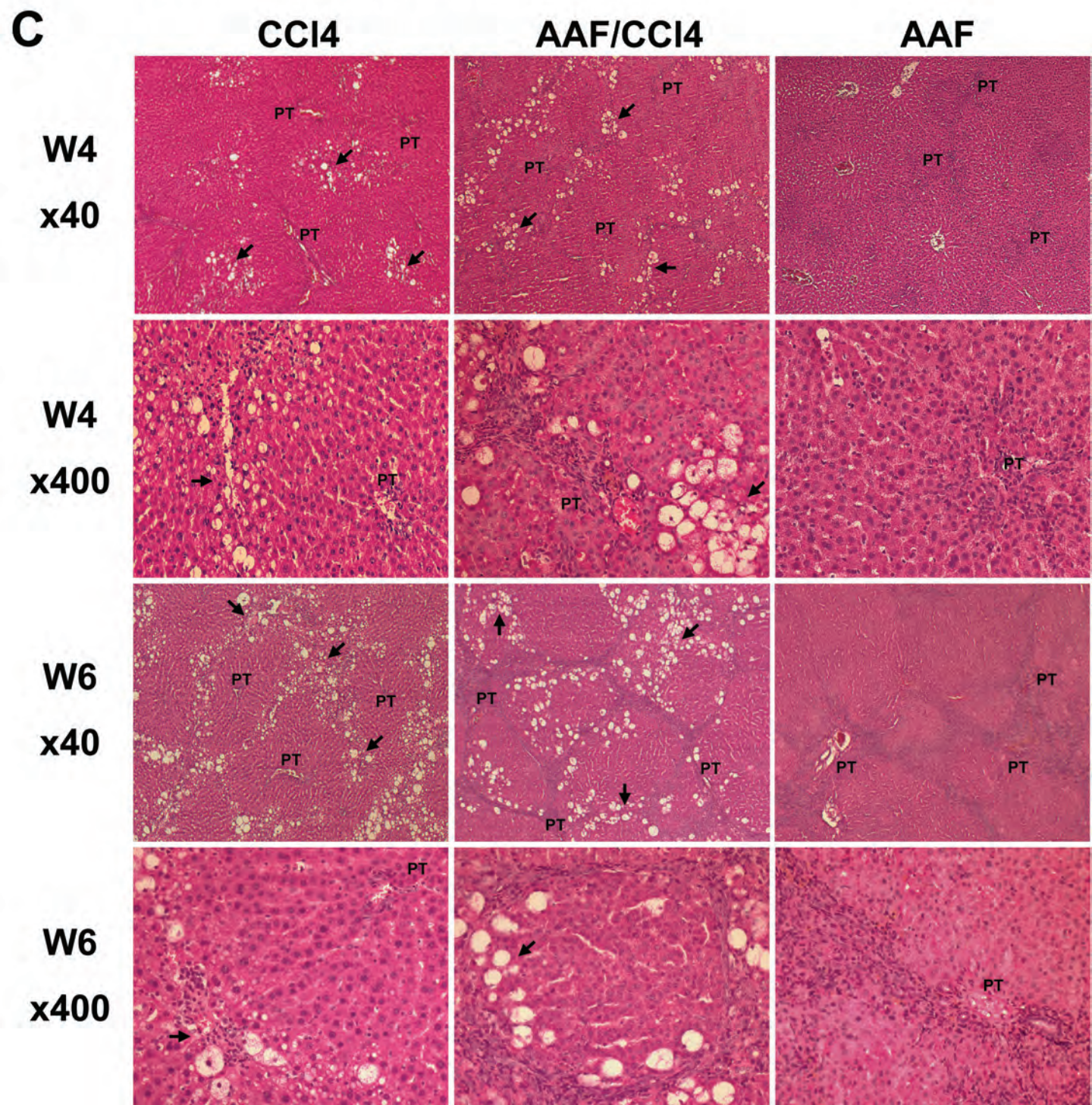
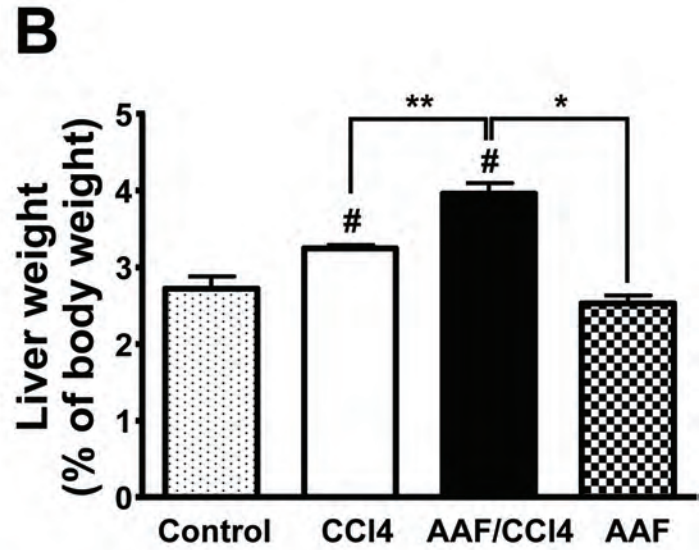
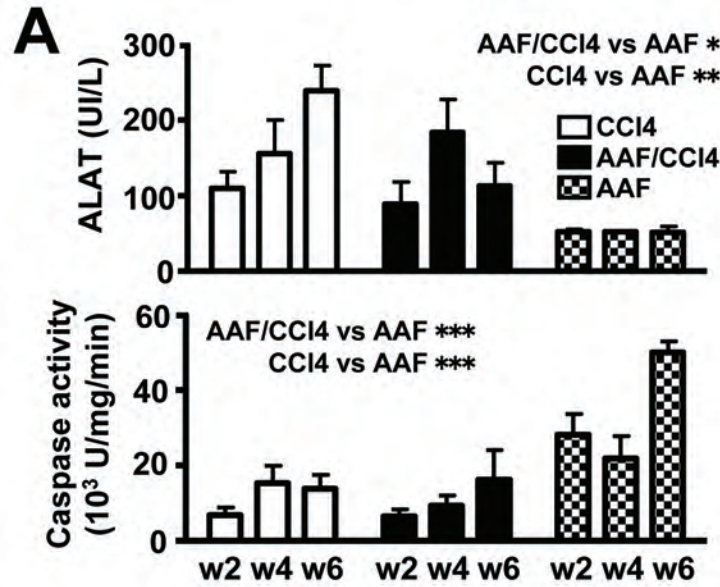
**Figure 7:** Immunolocalization of mesenchymal proteins on CK19-positive LPC from AAF/CCl<sub>4</sub>-treated animals after 6 weeks of treatment. **A)** Representative images of double immunofluorescence for CK19 (green) and myofibroblastic markers (red)  $\alpha$ SMA, desmin, FSP1 and collagen 1 of two experiments from two rats (original magnification x200). No merging signals between any mesenchymal marker and CK19

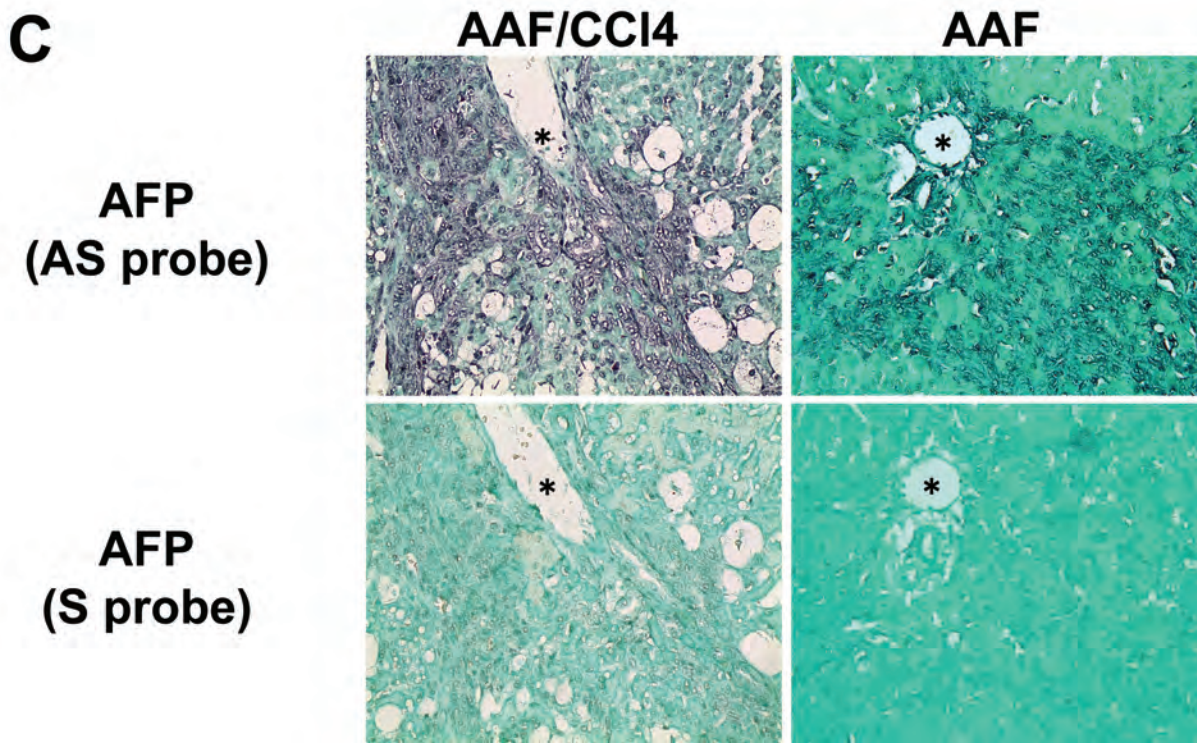
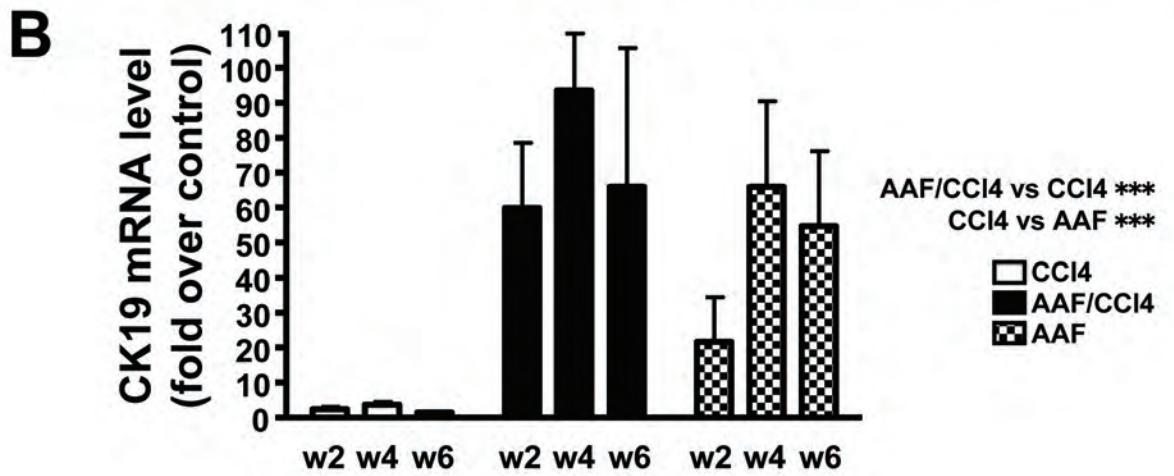
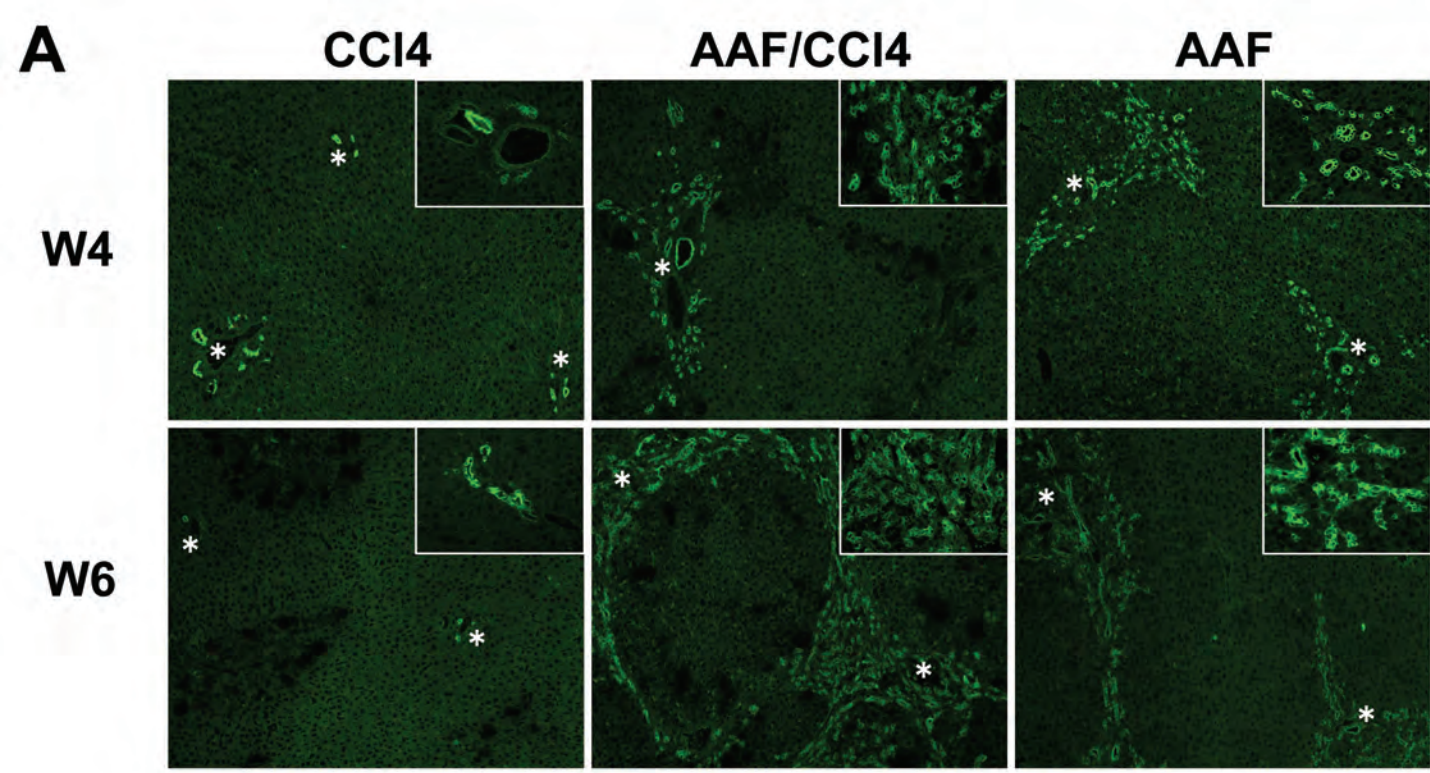
could be obtained in LPC. **B)** Confocal analysis confirmed the absence of mesenchymal markers in CK19-positive LPC that are surrounded by desmin- and  $\alpha$ SMA-positive cells (x630).

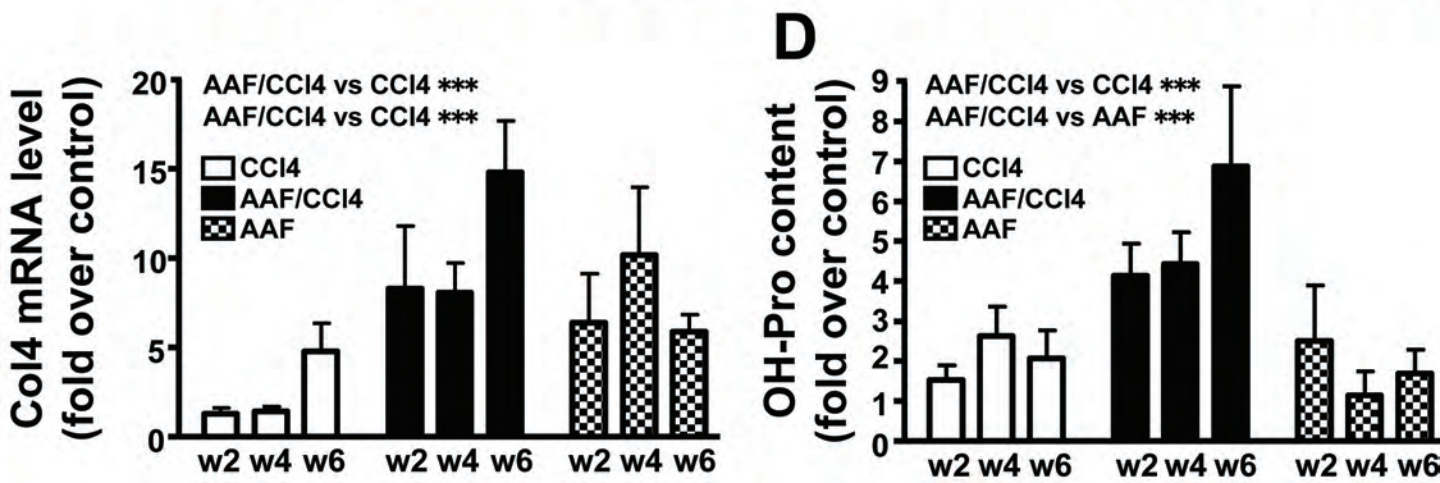
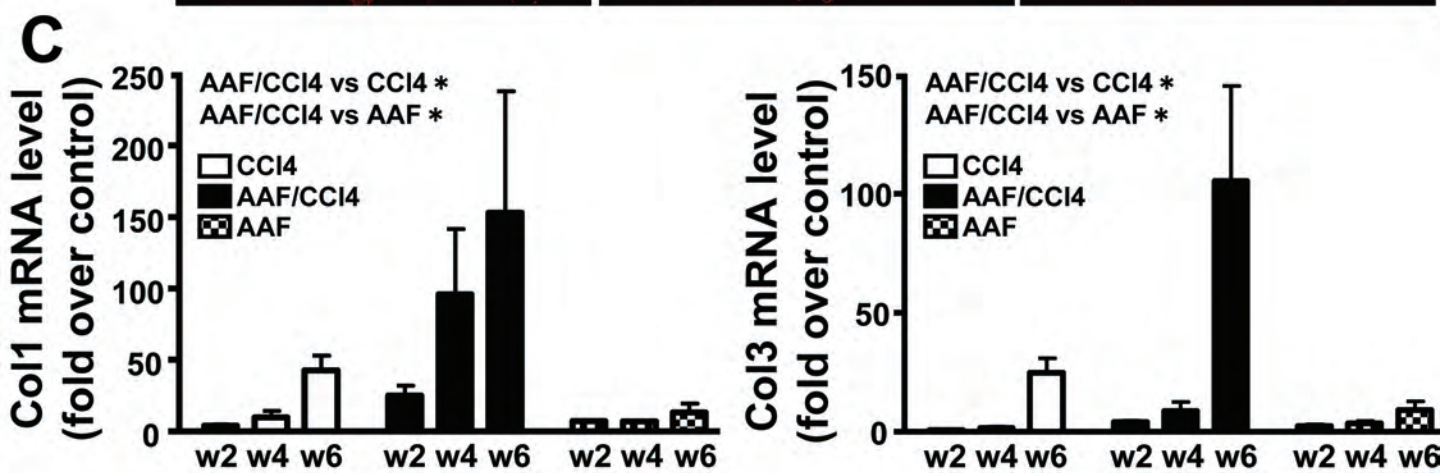
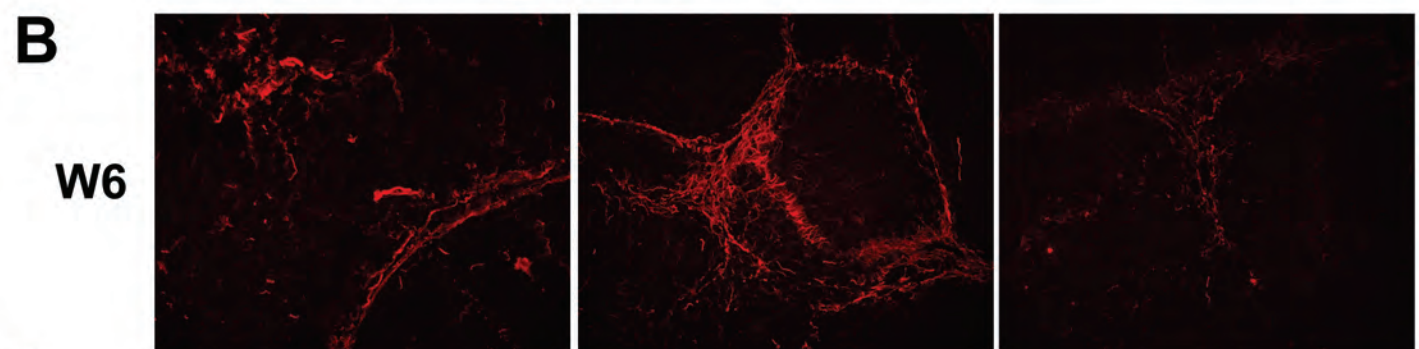
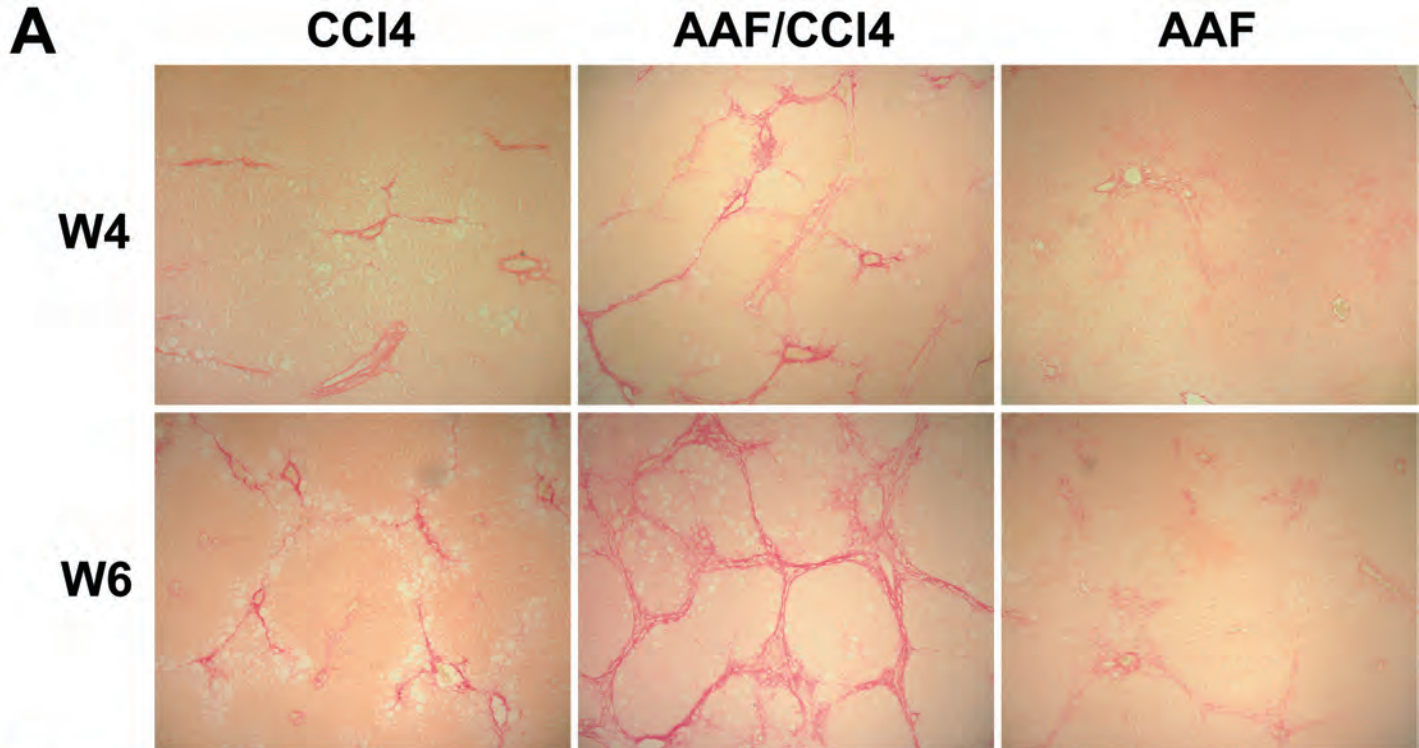
### Supplementary Figure Legends

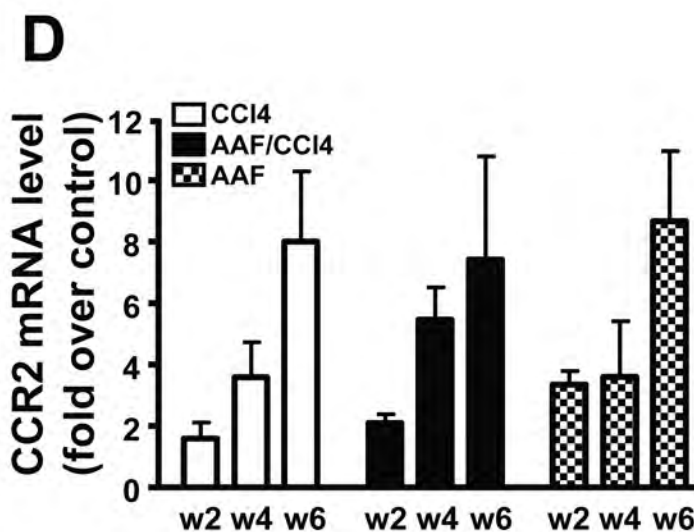
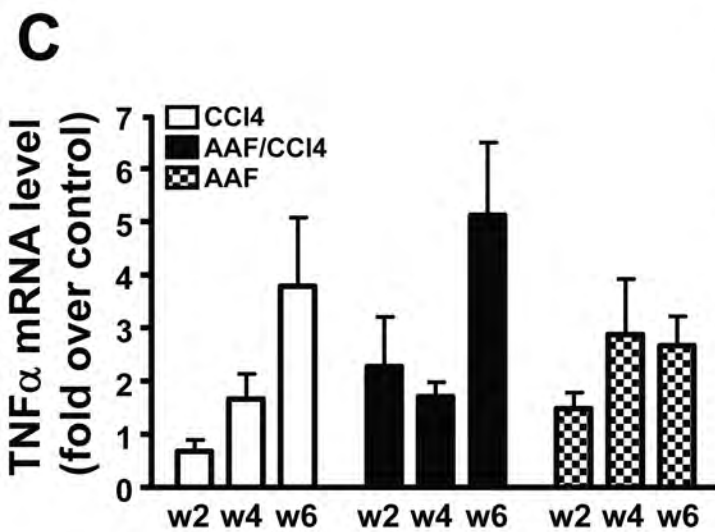
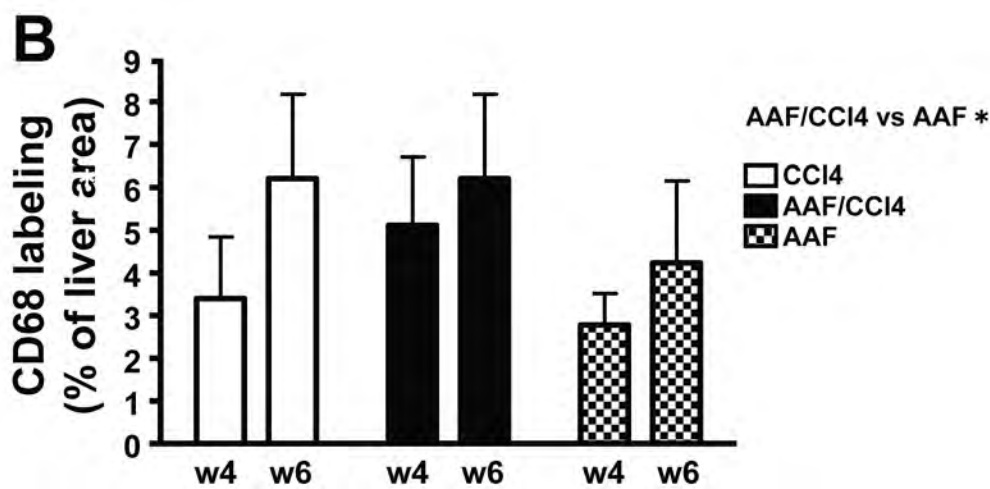
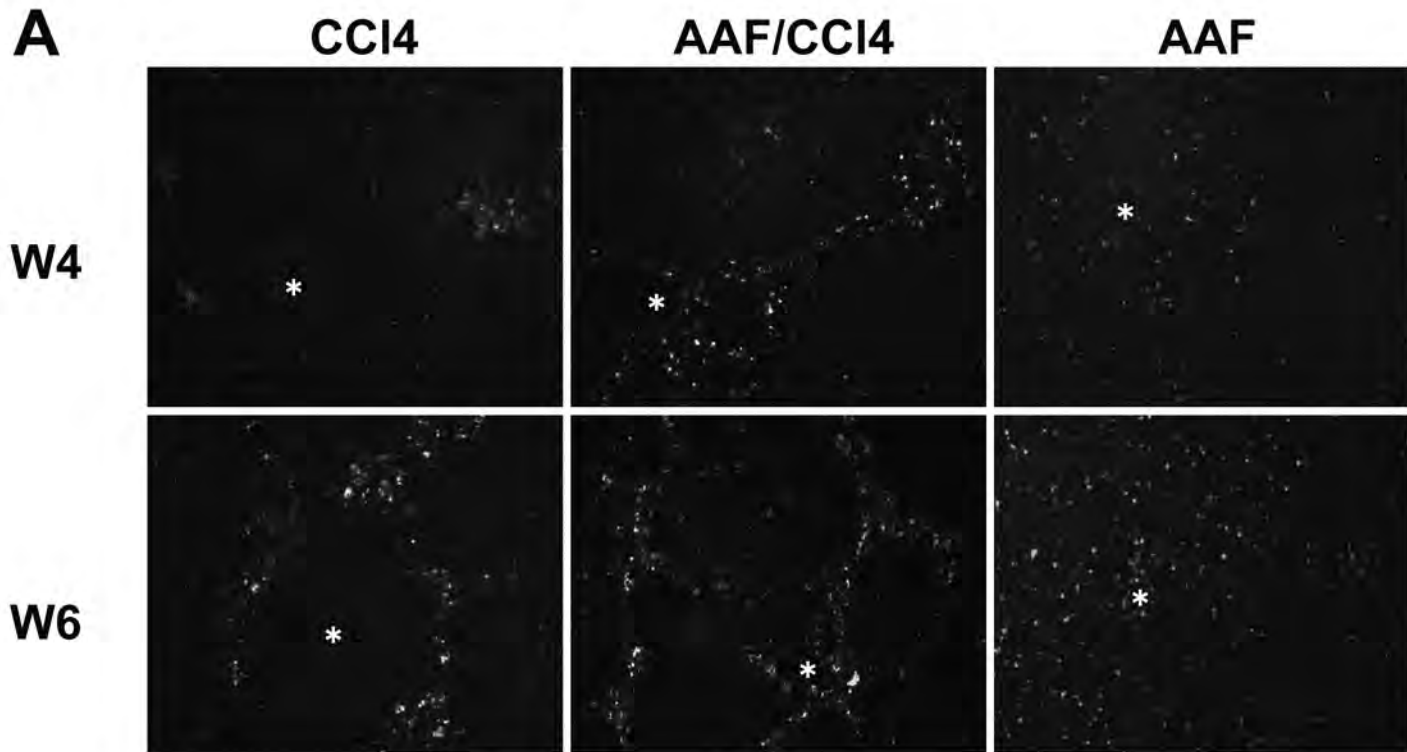
**Figure S1:** Representative photomicrographs (original magnification x200) on consecutive frozen liver sections and centered on the same area for CK19 staining (red) and *in situ* hybridization of AFP mRNA with nuclei counterstained with DAPI (blue). Lower panel at higher magnification (electronic zoom) evidenced AFP mRNA in CK19-positive cells from AAF/CCl<sub>4</sub>-treated animals.

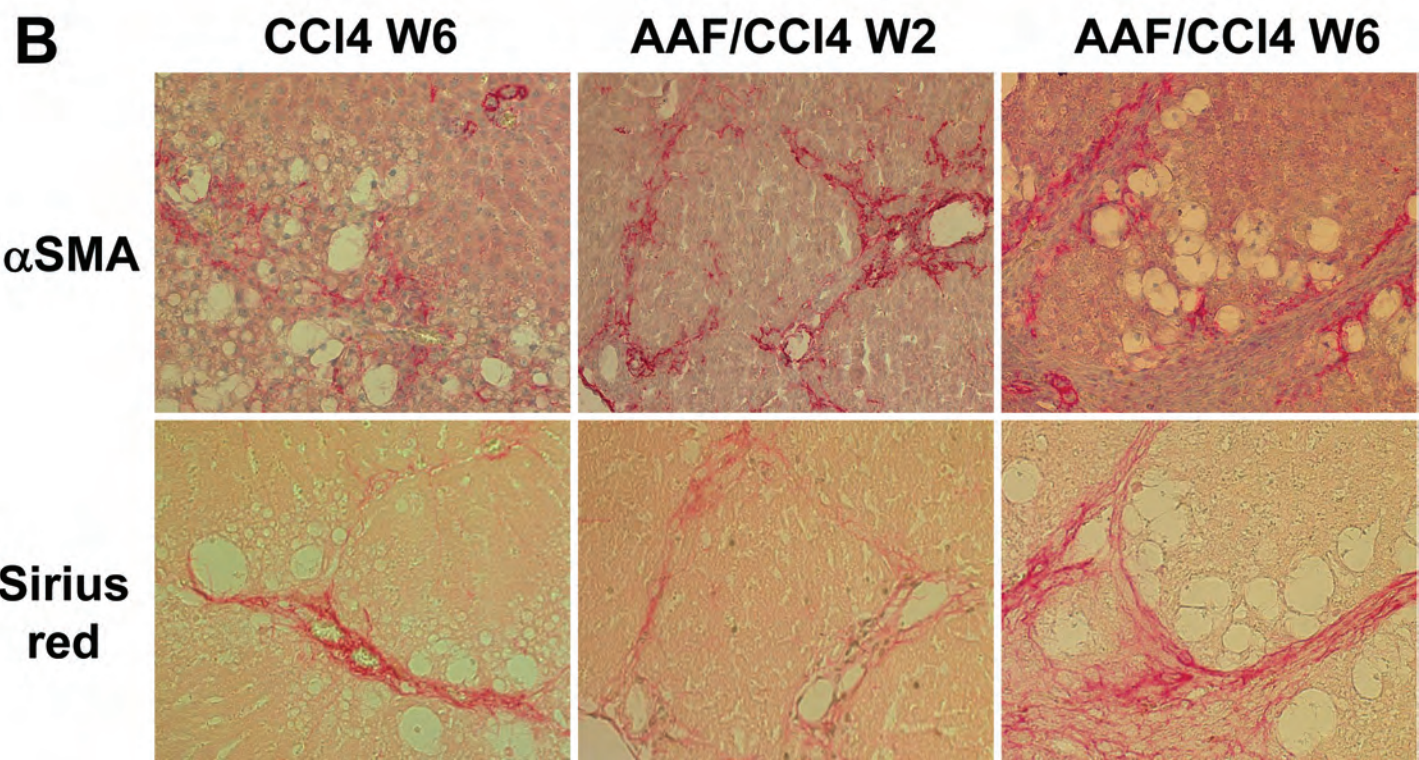
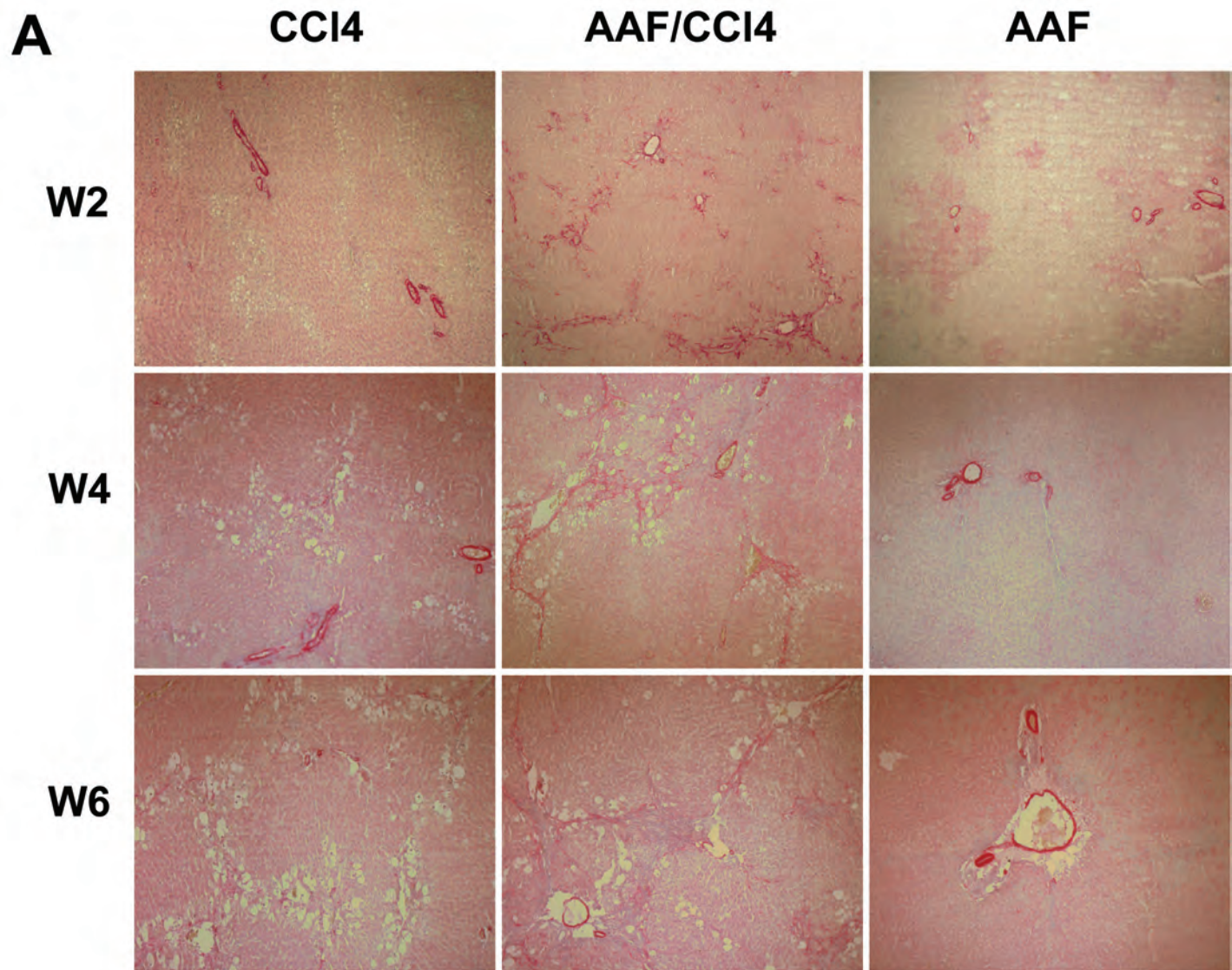
**Figure S2:** Representative photomicrographs (original magnification x200) on consecutive frozen liver sections and centered on the same area for CK19 staining (red) and detection of TGF $\beta$  mRNA by *in situ* hybridization with nuclei counterstained with DAPI (blue). Lower panel at higher magnification (electronic zoom) evidenced TGF $\beta$  mRNA in CK19-positive cells from AAF/CCl<sub>4</sub>-treated animals.

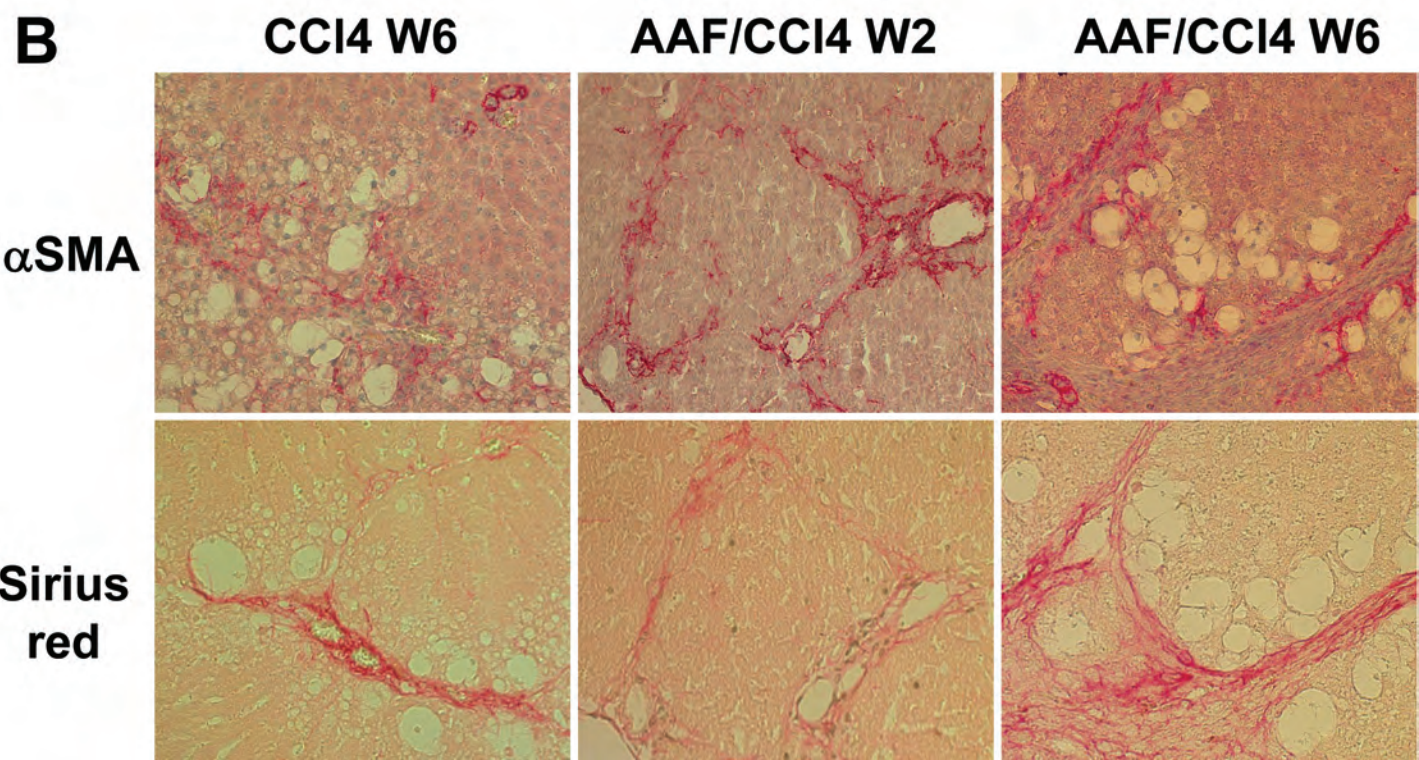
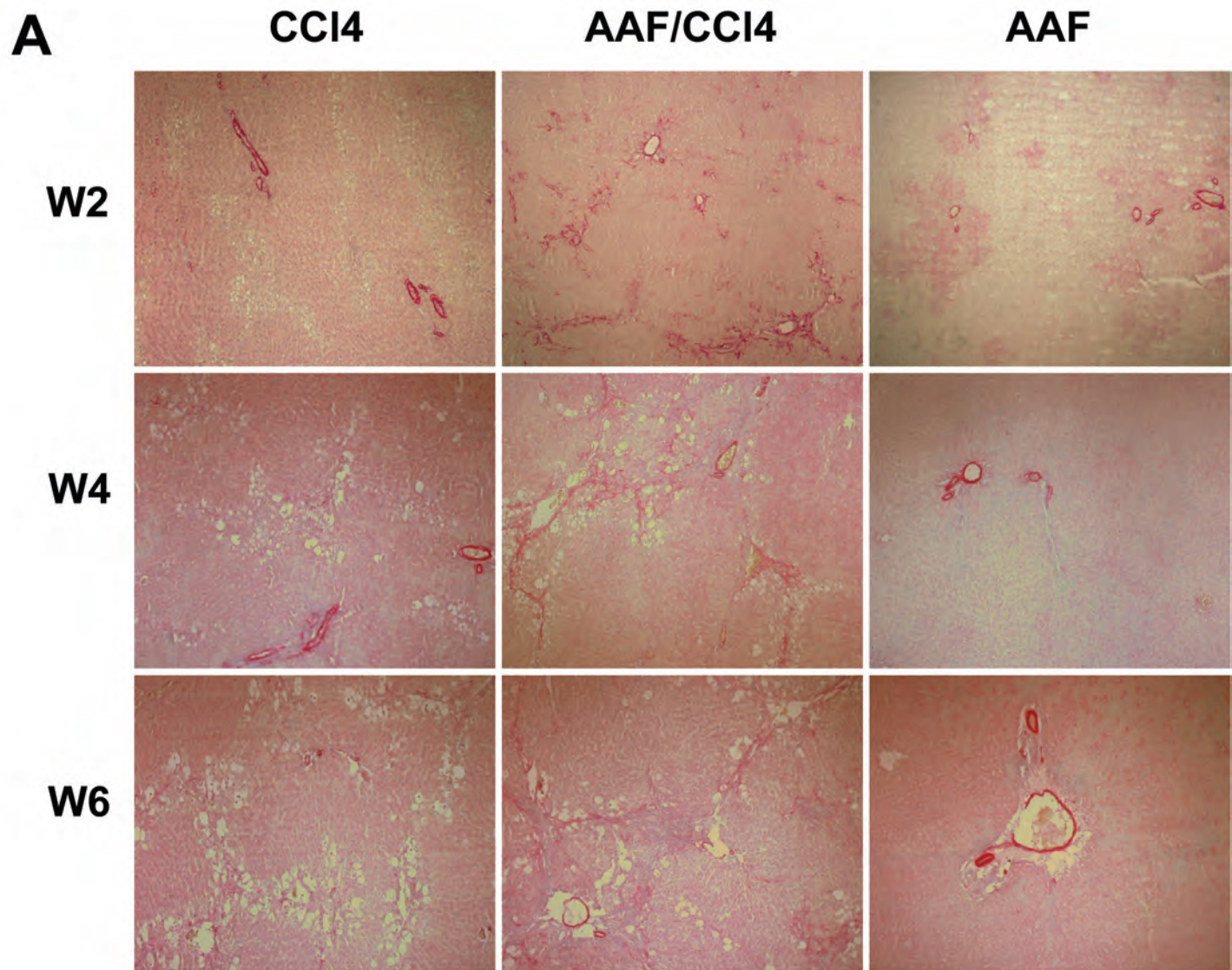


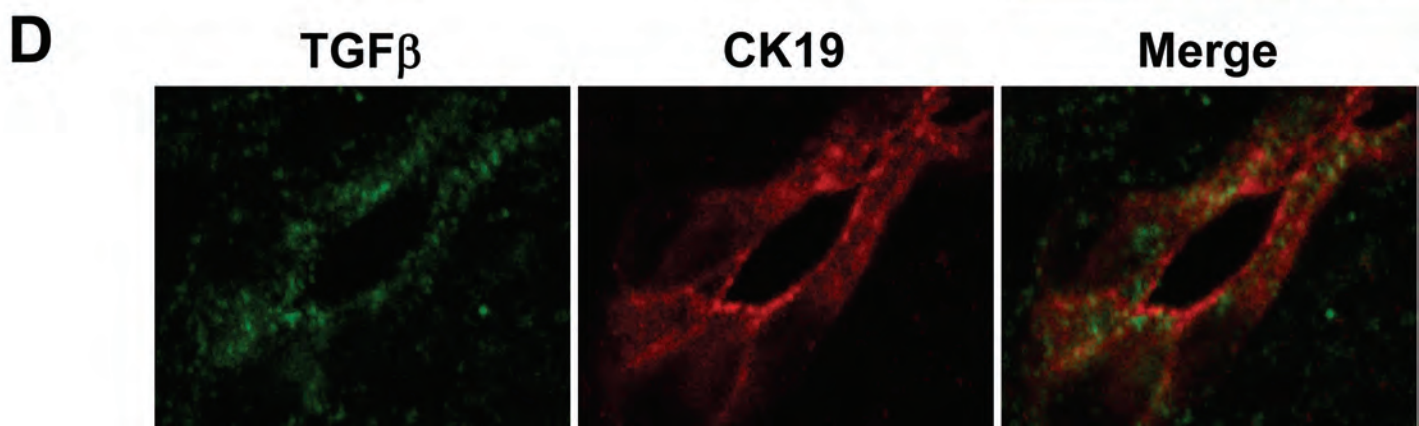
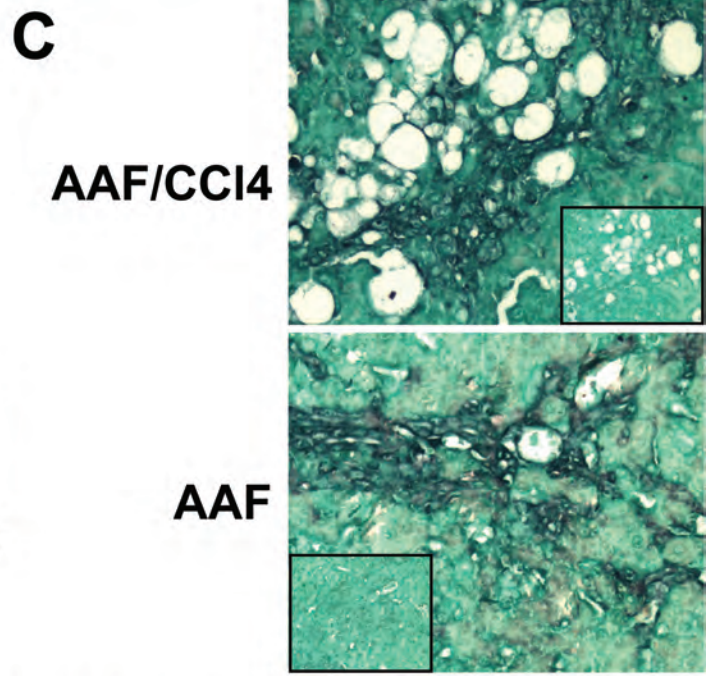
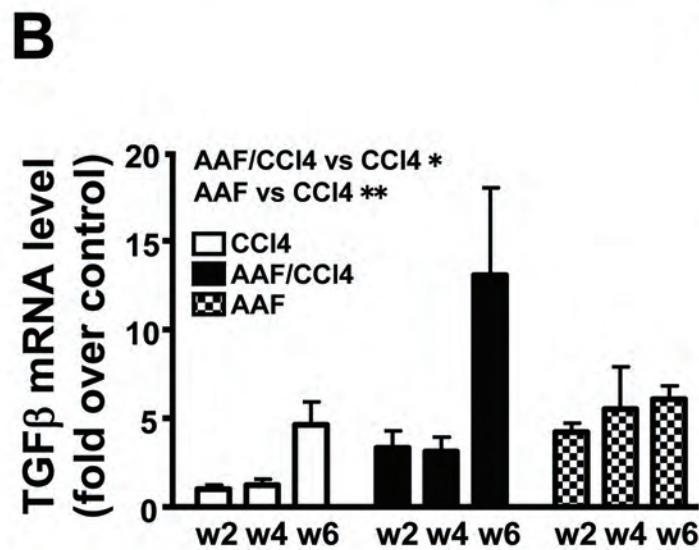
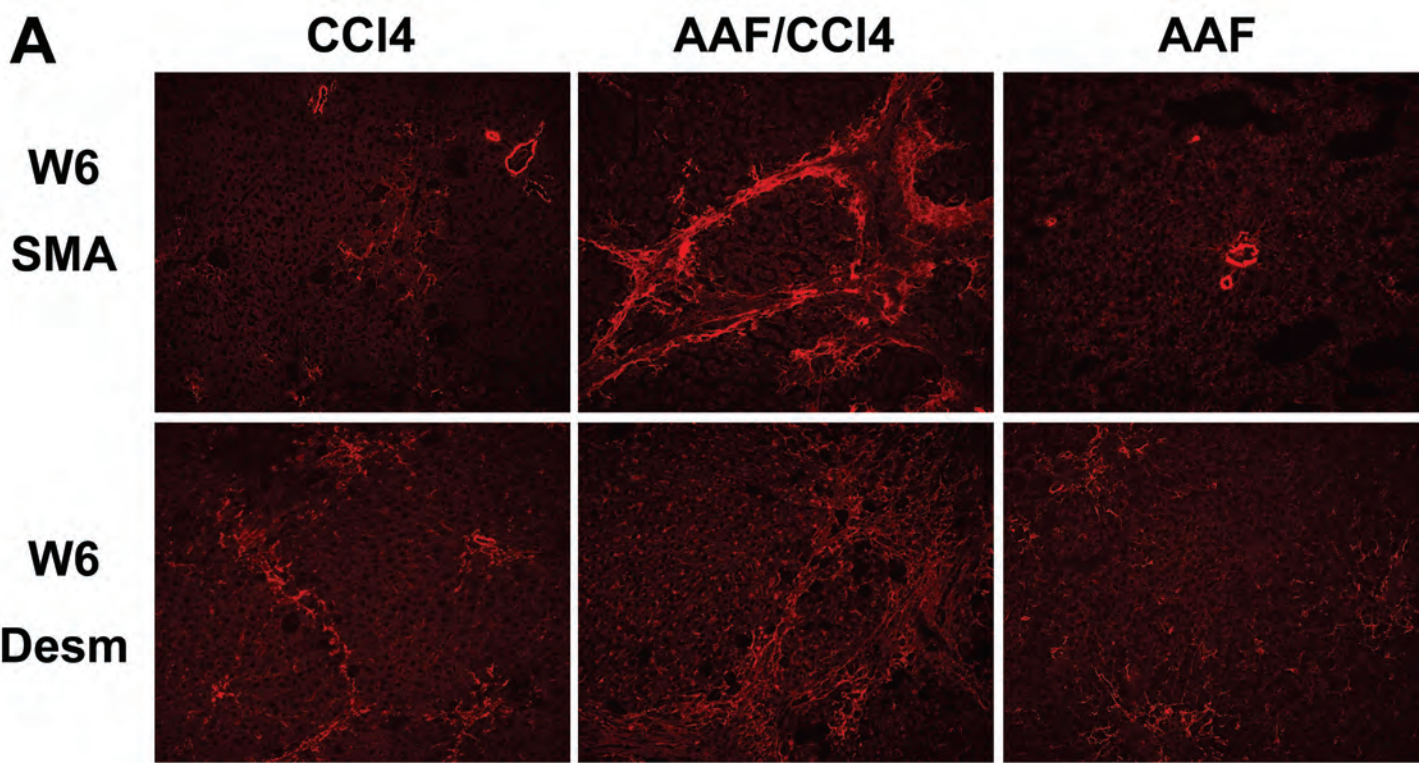


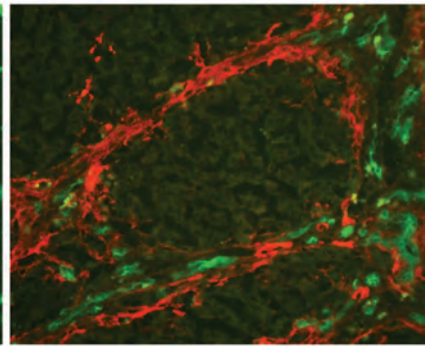
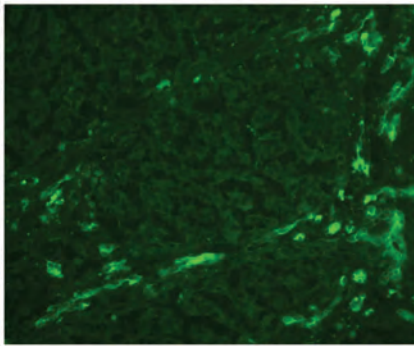
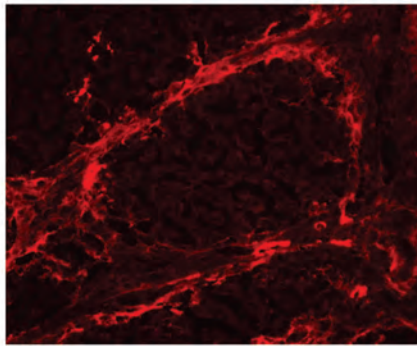
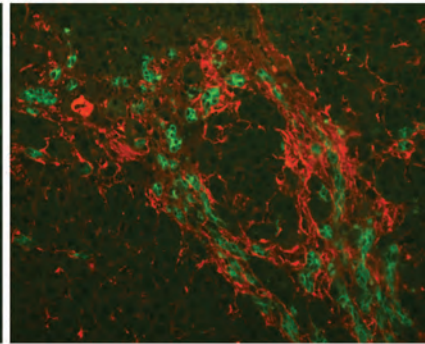
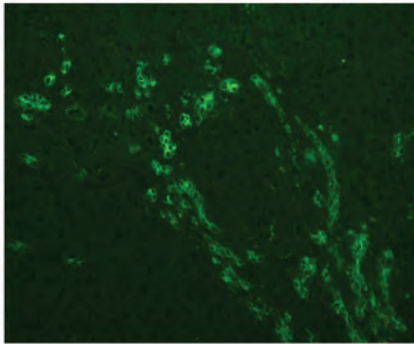
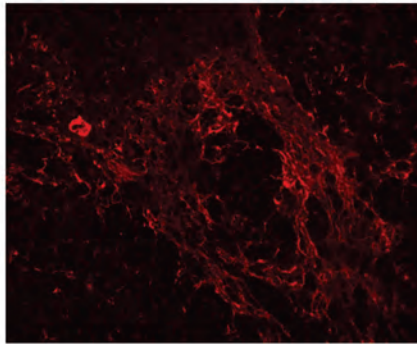
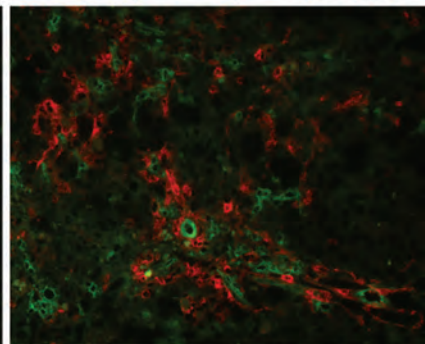
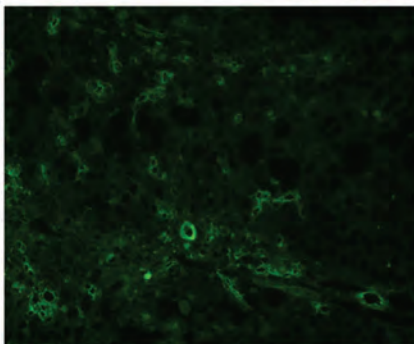
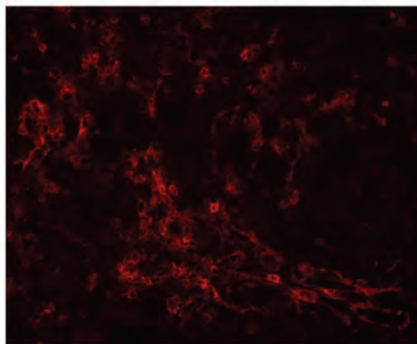
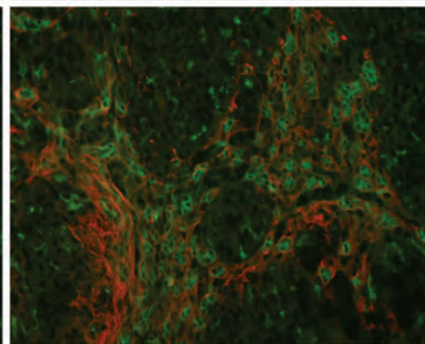
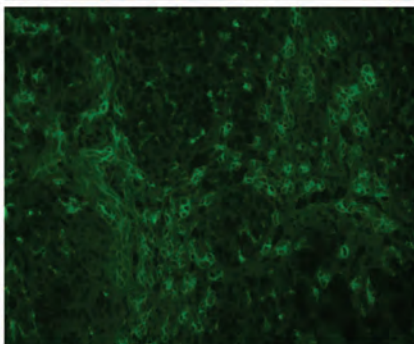
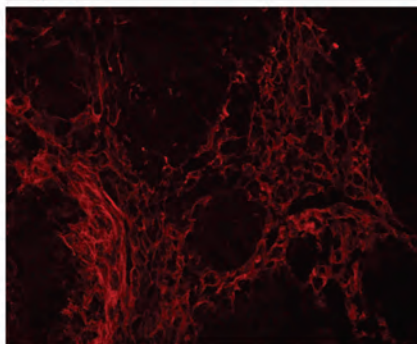
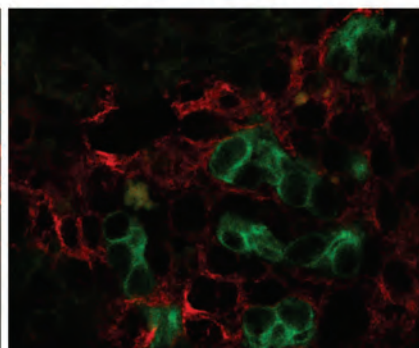
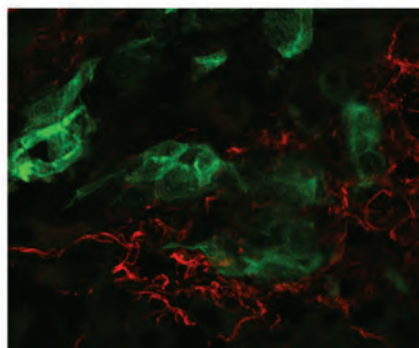


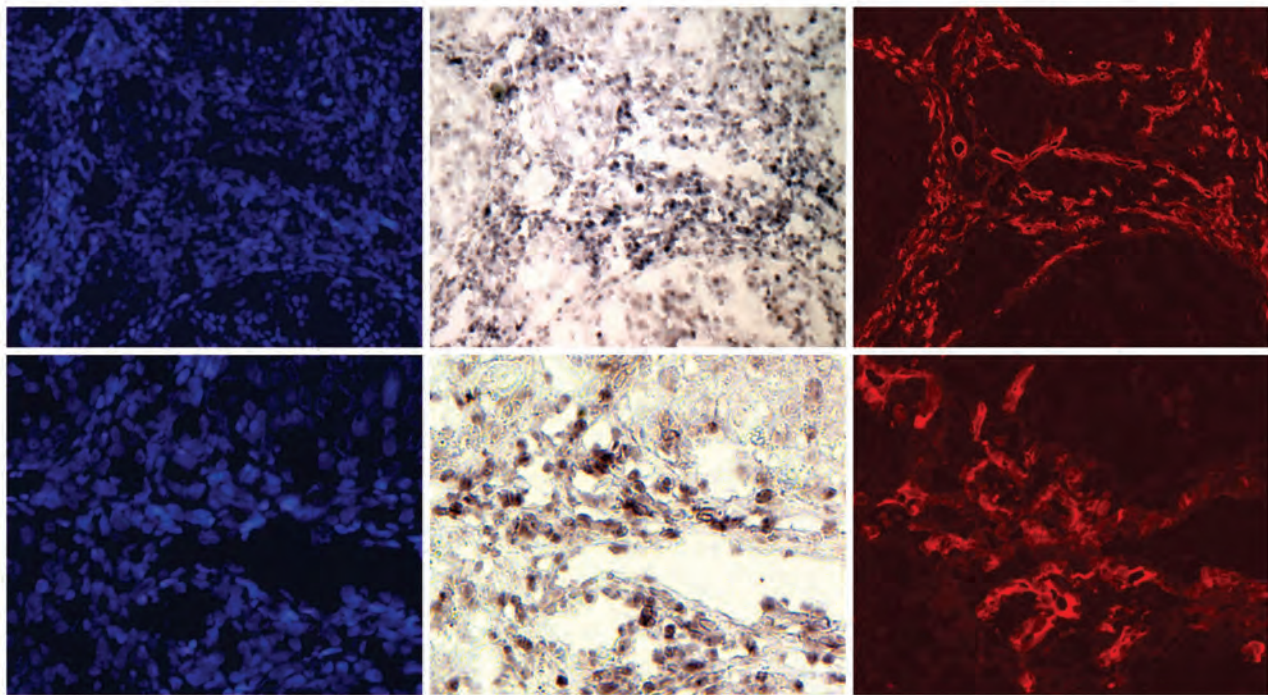




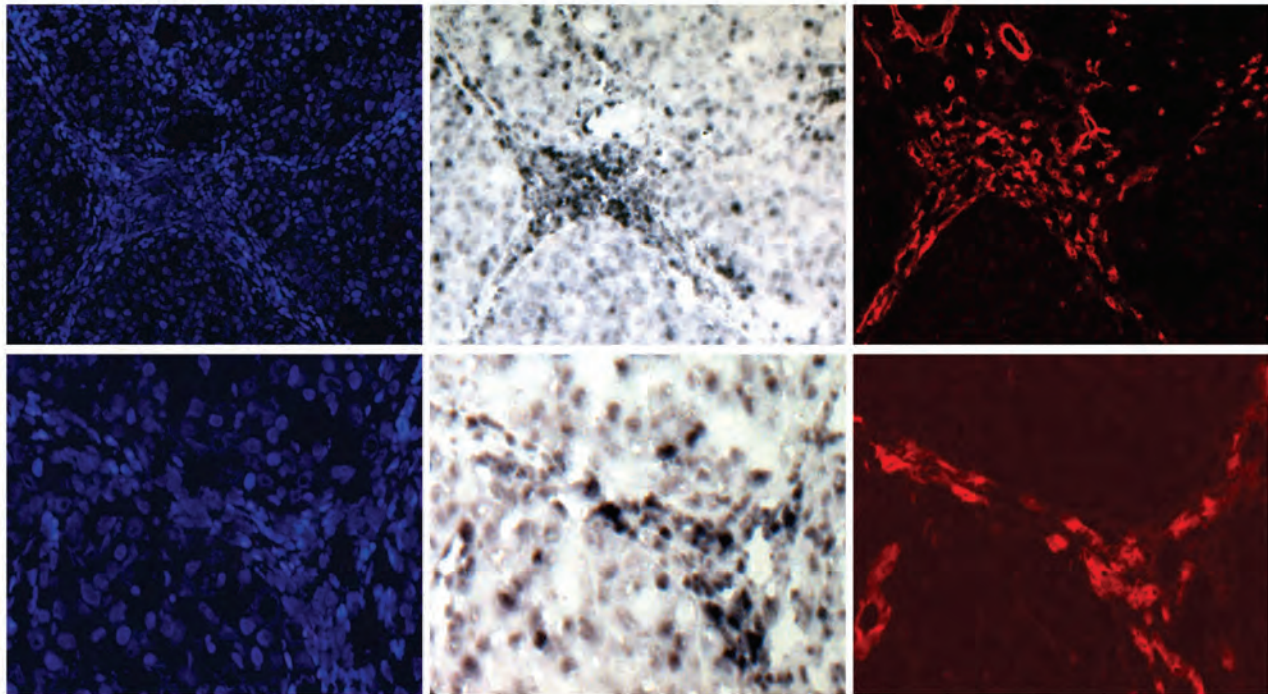




**A****CK19****Merge****SMA****Desm****FSP1****Col1****B****CK19/Desm****CK19/SMA**

**DAPI****AFP****CK19**

**Figure S1:** Representative photomicrographs (original magnification x200) on consecutive frozen liver sections and centered on the same area for CK19 staining (red) and in situ hybridization of AFP mRNA with nuclei counterstained with DAPI (blue). Lower panel at higher magnification (electronic zoom) evidenced AFP mRNA in CK19-positive cells from AAF/CCl<sub>4</sub>-treated animals.

**DAPI****TGF****CK19**

**Figure S2:** Representative photomicrographs (original magnification x200) on consecutive frozen liver sections and centered on the same area for CK19 staining (red) and detection of TGF $\beta$  mRNA by in situ hybridization with nuclei counterstained with DAPI (blue). Lower panel at higher magnification (electronic zoom) evidenced TGF $\beta$  mRNA in CK19-positive cells from AAF/CCl $_4$ -treated animals.